Tectonophysics 518–521 (2012) 1–16

Contents lists available at SciVerse ScienceDirect

Tectonophysics

journal homepage: www.elsevier.com/locate/tecto

Uniform basin growth over the last 500 ka, North Anatolian Fault, Marmara Sea, Turkey

Christopher C. Sorlien [a,e,*], Selin D. Akhun [b], Leonardo Seeber [c], Michael S. Steckler [c], Donna J. Shillington [c], Hülya Kurt [d], Günay Çifçi [b], Duygu Timur Poyraz [d], Savaş Gürçay [b], Derman Dondurur [b], Caner İmren [d], Emre Perinçek [d], Seda Okay [b], H. Mert Küçük [b], John B. Diebold [c]

[a] Earth Research Institute, University of California at Santa Barbara, Santa Barbara, USA
[b] Institute of Marine Sciences and Technology, Dokuz Eylül University, Izmir, Turkey
[c] Lamont-Doherty Earth Observatory, Columbia University, Palisades, NY, USA
[d] Department of Geophysics, Istanbul Technical University, Turkey
[e] Department of Earth Science, University of Missouri, USA

ARTICLE INFO

Article history:
Received 25 May 2011
Received in revised form 3 October 2011
Accepted 8 October 2011
Available online 15 October 2011

Keywords:
Transform basins
Seismic stratigraphy
North Anatolian Fault
Marmara Sea Turkey
Evolution strike-slip fault

ABSTRACT

Much of the northern strand of the North Anatolia Fault system in the Marmara Sea, the Main Marmara fault, is a seismic gap, posing a high risk for Istanbul. Deep bathymetric and sedimentary basins are structurally associated with the Main Marmara fault. Basin growth including tilting of their margins is thus linked to fault slip through releasing and restraining segments of this and other branches of the North Anatolian Fault system. Whether this system has been steady state through at least the last half of the Quaternary, or whether the Main Marmara fault more recently propagated through and deactivated pull-apart basins is one of the main controversies.

A published age model and stratigraphic framework for these basins has been lacking, and tectonic history models for the Marmara Sea have relied on extrapolating present deformation rates back through time. Over 3000 km of new high-resolution multichannel seismic reflection combined with existing lower-resolution seismic reflection and multibeam bathymetric data make possible a detailed regional stratigraphic interpretation. In particular, a stack of shelf-edge deltas are imaged, and interpreted as glacial period deposition during low sea/lake levels. Reflections from the tops of these deltas, and from unconformities were correlated across much of Marmara Sea basins and highs, providing critical stratigraphic control.

We correlate the low-stand deltas with known eustatic sea level minima by developing proxies for time from vertical separation of strata across normal faults, tilts, and sedimentary volumes. A preferred age model is proposed at least back to Oxygen Isotopic stage 14 at 536 ka. During this time interval, tilting of basin margins, vertical separation across the Main Marmara fault adjacent to western Istanbul, and tilt-related slow collapse on the south flank of the Çinarcik basin all indicate steady-state basin growth and fault slip.

1. Introduction

For most of its 1500-km length, the North Anatolian Fault (NAF) system is a relatively simple and narrow fault zone that carries almost all of the current and cumulative right-lateral displacement of the plate boundary between Eurasia and the Anatolian block. However, in its western part, the North Anatolian Fault system splays into several branches, each made up of discrete strands. At the longitude of Istanbul the splays are distributed N–S across an 80 km belt (Fig. 1). Here, in northwestern Turkey, a composite transtensional basin formed along the NAF system. The Marmara Sea overlies this basin. The northern branch of the NAF, also called the Main Marmara Fault (Le Pichon et al, 2001) is associated with three 1200-m-deep bathymetric basins in the Marmara Sea (from west to east: Tekirdağ, Central and Çinarcik Basins; Fig. 1) in which the base of Neogene sedimentary rock may be as deep as 6 km (Armijo et al., 1999; Bécel et al., 2010; Carton et al., 2007; Laigle et al., 2008). The Main Marmara fault connects from the Izmit fault in the east to the Ganos fault in the west (Fig. 1).

GPS data indicate 23–25 mm year of displacement across the plate boundary through northwest Turkey (Le Pichon et al., 2003; McClusky et al., 2000; Meade et al., 2002; Reilinger et al., 1997), while paleoseismic studies suggest a slower Holocene rate of 10 mm/yr (Polonia et al., 2004) or late Holocene rate of ~20.5 mm/yr (Kozaci et al., 2007). The accumulating strain was relieved in part by the 20th century series of major and deadly earthquakes that progressed from east to west

* Corresponding author.
E-mail address: sorlien@eri.ucsb.edu (C.C. Sorlien).

0040-1951/$ – see front matter © 2011 Elsevier B.V. All rights reserved.
doi:10.1016/j.tecto.2011.10.006

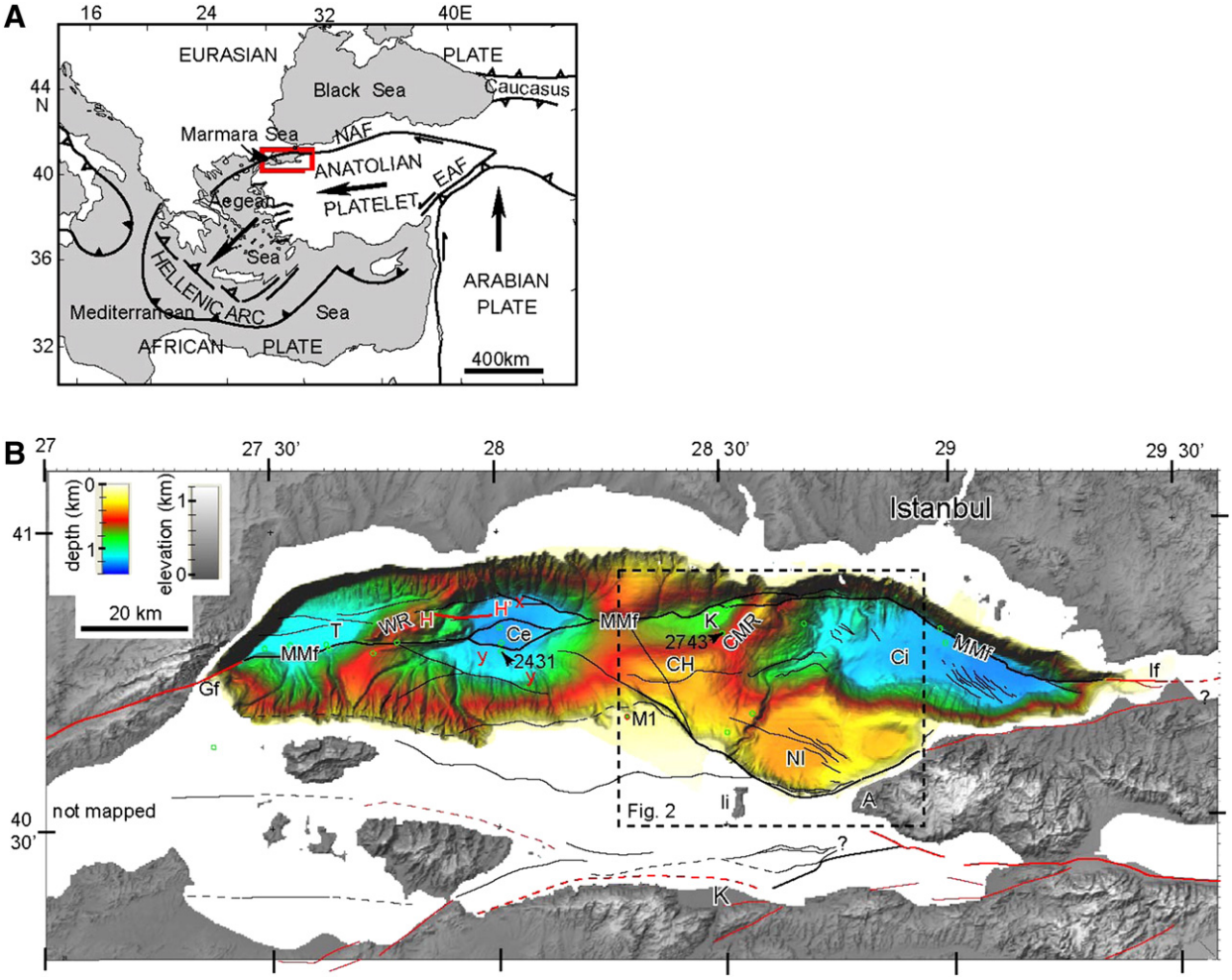

Fig. 1. A: Eastern Mediterranean tectonics, modified from Okay et al. (2000). "B" located by red rectangle. NAF = North Anatolian fault. B: Faults, bathymetry, topography for Marmara Sea. Three ~1200 m-deep basins are arrayed along the Main Marmara fault. Bathymetry from Rangin et al. (2001); We mapped faults in black; faults in red from published sources compiled by Erturaç (2002); including Okay et al (2000); Kazanci et al. (1999), Kuşçu et al., 2009), Barka (1999); Cormier et al. (2006); and Parke et al. (2002). Green circles are locations of cores from R.V. Marion du Fresne 2001 and 2004 (Beck et al., 2007; Lericolais and Henry, 2004).Gf = Ganos Fault; If = Izmit fault; M1 = Marmara 1 well; MMf = Main Marmara fault; T = Tekirdağ basin; Ce = Central Basin, K = Kumburgaz basin; Ci = Çinarcik basin; NI = North İmrali basin; CH = Central High; CMR = Central Marmara Ridge; WR = Western Ridge; Ii = İmrali Island; A = Armutlu Peninsula, and K = Kocasu River delta. In Central basin: x = sea floor scarp, and y = onlap.

(Barka, 1996; Stein et al., 1996; Toksoz et al., 1979), leaving a long segment within Marmara Sea near Istanbul as a seismic gap. This gap has not broken since 1766 (Armijo et al., 2005; Barka, 1996; Le Pichon et al., 2003). Furthermore, it has been proposed that part of seismic gap has not broken since 1509, with a shorter segment possibly not breaking even in 1509 (Ambraseys and Finkel, 1995; Ambraseys and Jackson, 2000).

An international effort to image the sea floor and sub-bottom of Marmara Sea over the last decade was further motivated by the destructive and deadly 1999 earthquakes in the easternmost Marmara Sea in the Gulf of Izmit and east of there. Istanbul is built along the shores of Marmara Sea and the hazard and risk from earthquakes to it and its over 13 million residents over the next decades is extremely high (Hubert-Ferrari et al., 2000; Parsons, 2004; Parsons et al., 2000). Models of and forecasts for future earthquakes are uncertain, however, because of large uncertainties persisting on the fault structure and evolution. For example, it is uncertain whether the structure of the fault zone responsible for the basins is still active in a steady-state mode (Armijo et al., 1999, 2002; Seeber et al., 2004, 2010), or if it has been replaced in recent geologic time by a simpler fault geometry that cuts through pull-apart basins and fosters pure dextral motion along a continuous fault. This dispute is relevant to the potential for a single rupture across the entire Marmara seismic gap vs. several smaller ruptures (Le Pichon et al., 2003; Rangin et al., 2004; Sengör et al., 2005).

These questions highlight that "establishment of a good stratigraphy of these basins is one of the most urgent tasks to progress in the understanding of the tectonic history" (İmren et al., 2001). To address this problem, we undertook a 3-week cruise on board the R/V K. Piri Reis in 2008 with a short follow-up cruise in 2010. The high-resolution multichannel seismic (MCS) data collected images the upper 1–2 km of the strata in sufficient resolution for sequence stratigraphic interpretation. This was facilitated by the discovery of a stack of lowstand deltas in the North İmrali basin in the southern Marmara Sea (Fig. 1). Using these data, this paper develops a late Quaternary (last ~800 ka) stratigraphic age model for North İmrali basin), and then correlates this stratigraphy to other transform basins along the Main Marmara fault. Thus, fault and basin evolution in the Marmara Sea can be quantitatively examined for the first time, and the backward extrapolation of GPS velocity can be tested, rather than used as an assumption. Our stratigraphic model and correlations support steady-state growth of basins and of the vertical component of motion across a restraining segment of the Main Marmara fault.

2. Kinematic models

Over the past decades, the numerous geophysical surveys, including deep multichannel seismic reflection surveys, and shallow single channel chirp, and sparker seismic reflection surveys, together with multibeam bathymetry, have been used to map the major sedimentary basins and surface fault patterns of the Marmara Sea. However, differing interpretations of the relationships of the various structures have resulted in multiple models for the evolution of the Marmara Sea basins and their current relationship to the NAF. Among the many models that have been proposed, the recent models can be grouped into three types:

Steady-state 1: The major deep-water basins formed as pull-apart basins linked by short strike-slip segments (e.g., Armijo et al, 1999, 2002; Barka and Kadinsky-Cade, 1988).

Steady-state 2: The Tekirdağ and Çinarcik Basins, at least, developed as asymmetric basins associated with bends in the major through-going strike-slip faults (Okay et al., 1999, 2004; Seeber et al., 2004, 2010).

Young reorganization 3: Accepts that the basins developed as the result of transtensional tectonics, but claims that the Main Marmara fault has cut through and deactivated the sedimentary basins (İmren et al., 2001; Kuşçu, 2009; Le Pichon et al., 2001, 2003; Rangin et al., 2004; Sengör et al., 2005).

Thus all models agree that extension or transtension is responsible for formation of the three ~1200 m-deep bathymetric basins, whose sedimentary fill is as deep as 6 km (Armijo et al., 1999; Bécel et al., 2010; Carton et al., 2007; Laigle et al., 2008). However, the models differ in the kinematics that produced the basins. Furthermore, these three basins are separated by two NE–SW structural ridges, the Western High and Central Marmara Ridge (Fig. 1). Depending on the model, these ridges are interpreted as either horsts (Aksu et al., 2000), or contractional anticlines (Okay et al., 1999, 2000; Rangin et al., 2004; Yaltirak, 2002). As a result of the ridges separating the basins, the stratigraphy within each basin has not been correlated to other basins, hampering efforts for a global evolutionary model.

The third model contrasts with the other two in that it proposes that the Main Marmara fault is a young feature, based on identified offset features. The Main Marmara fault appears to offset the Central Marmara Ridge dextrally by 3.5 km (Fig. 2; Armijo et al., 2002; Le Pichon et al., 2003). Using a range of slip rates of 10 mm/yr to the current maximum GPS deformation rate of 25 mm/yr on this strand produces an age of origin of 140,000 to 350,000 years (Armijo et al., 2002). In addition, back-slipping the Main Marmara fault by 4 km restores Central Basin to a symmetric shape. This yields a similar age of formation for this strand of 200,000 ± 100,000 years (Le Pichon et al., 2003; Rangin et al., 2004; Sengör et al., 2005). Furthermore, it is proposed that following this young formation of the Main Marmara fault, only pure strike-slip, with transpression across E–W segments of the Main Marmara fault has been occurring (Demirbağ et al., 2003; İmren et al., 2001; Le Pichon et al., 2001; Rangin et al., 2004). In these models, basin-bounding normal faults were active, with the basins extending and subsiding, mainly before formation of the Main Marmara fault. Now most of the motion is focused on the almost pure transform Main Marmara Fault and basin growth is slowed to stopped. Ongoing partitioned normal slip on shorter faults is interpreted near a Main Marmara fault bend in southeast Çinarcik basin (e.g., Le Pichon et al., 2003).

In contrast, Seeber et al (2004) have interpreted a uniform and rapid rate of subsidence and tilt above a non-vertical Main Marmara Fault segment back to 1.4 Ma in the western (Tekirdağ) basin. A smoothly increasing vertical component of slip with depth is imaged to the base of 5 km-deep sedimentary fill across the Main Marmara

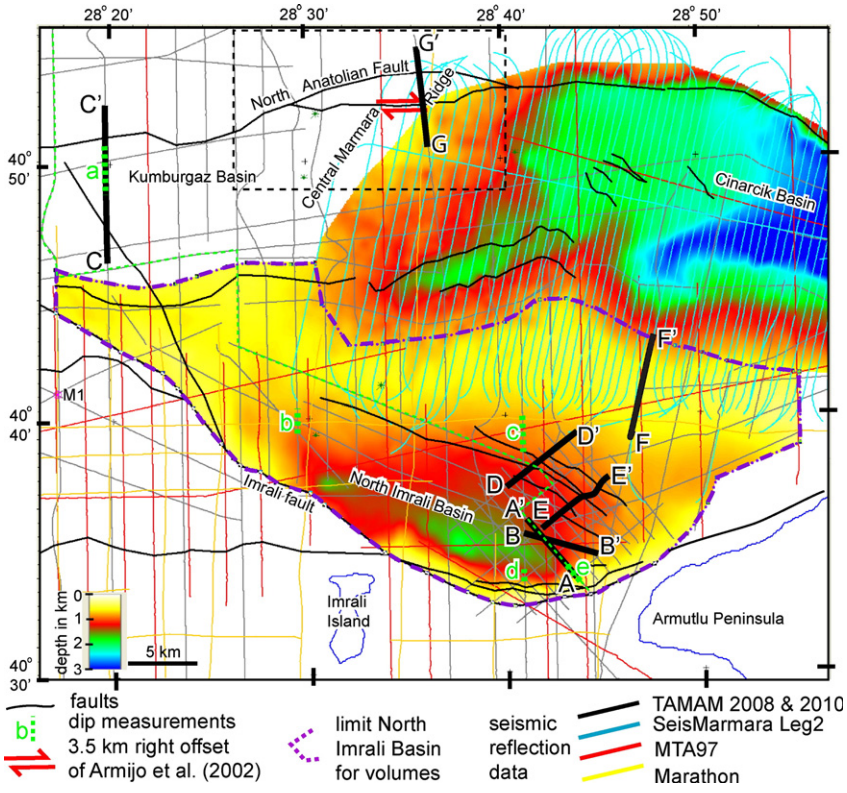

Fig. 2. Tracklines of the seismic reflection data sets plotted as color lines, identified in the legend. Area used for volumes of intervals between delta horizons outlined (dashed-dotted violet); dip measurement locations (dotted green line segments labeled "a" through "e"); heavy black lines indicate profiles in other figures), and light green dotted line indicate the regional correlation profile in Fig. 6. The background to this Figure is the depth of the Green-6 horizon. The 3.5 km right offset of Central Marmara Ridge (Armijo et al., 2002) is located at the paired heavy red arrows.

Fault in Central Basin, consistent with steady-state kinematics there during at least the last 1 m.y. and probably several m.y. (Laigle et al., 2008). Alternatively, Armijo et al. (1999, 2002), interpret continuing pull-apart activity with transtension across E–W fault segments.

The lack of age control earlier than 40 ka in the deep basins makes it difficult to evaluate whether or not there has been a dramatic change in the rate of basin growth over the last few hundred thousand years. The problem is exacerbated by the lack of stratigraphic correlation between the basins. To address this problem, we undertook high-resolution multichannel seismic reflection surveys to better image the basin stratigraphy and to correlate that stratigraphy between basins. We combine these data with considerable existing data in order to search for evidence of the proposed young reorganization.

3. Data

Multibeam bathymetry data were recorded across all of the deeper parts of the Marmara Sea, and are publicly available (Le Pichon et al., 2001; Rangin et al., 2001). Several very high-resolution chirp, and sparker single-channel surveys have imaged the shallow subsurface (Aksu et al., 1999; Gökaşan et al., 2010; Smith et al., 1995).

The TAMAM (Turkish American MArmara Multichannel) Project undertook two cruises (Fig. 2) using the R/V *K. Piri Reis*, operated by the Institute of Marine Sciences and Technology of Dokuz Eylül University. During the first cruise in 2008, we acquired 2700 track-km of high-resolution 72-channel seismic reflection and chirp seismic data throughout the Sea of Marmara. In a follow-up cruise in 2010 we filled in data gaps due to heavy traffic in the shipping lanes and collected targeted lines necessary for correlations between basins. TAMAM 2010 acquired 298 track-km of 240- or 111-channel data (acquisition parameters are summarized in Table 1). The shallow towing of the source and streamer facilitated high-frequency records for imaging the stratigraphy because the 'ghost' arising from the reflection of the source wave off the water surface occurs at 250 Hz and 187.5 Hz for 3 and 4 m tow depths, respectively, thus preserving a large range of high frequencies. Processing of the multichannel seismic reflection (MCS) data used standard steps including detailed velocity analysis and post-stack time migrations. Finite difference post-stack depth migration was performed on a few profiles (e.g. Fig. 3).

These data were supplemented by additional existing MCS data including 1500 km of migrated profiles recorded by MTA in 1997 (İmren et al., 2001; Okay et al., 1999, 2000). We used these data as processed by Parke et al. (2003). In addition, graphics files of 948 km of 12 and 24-fold non-migrated low resolution profiles recorded in 1972 and 1973 (C&K Petroleum, 1974) were converted to SEGY format, plus migrations of 83 profiles totaling over 2000 km of deep-penetration, low resolution SEISMARMARA Leg 2 profiles were also available for this study (Fig. 2; published in Carton et al, 2007). This combined data set, along with a 20 m grid of multibeam bathymetric data recorded across all of the deeper parts of the Marmara Sea (Le Pichon et al., 2001; Rangin et al., 2001), were imported into the industry seismic reflection interpretation software "The Kingdom Suite".

Table 1
General shooting and recording parameters for the 2008 and 2010 TAMAM surveys. GI: Generator-injector airgun.

Parameters	2008	2010
Number of channels	72	111 or 240
Streamer length (m)	450	750 or 1500
Near offset (m)	40 or 100	15 or 64
Far offset (m)	493 or 543	760 or 1557
Shot interval (m)	12.5 or 18.75	18.75
Group interval (m)	6.25	6.25
Sampling (ms)	1	1
Record length (s)	4	5
Maximum fold	12 or 18	18 or 40
Source	1 45 + 45 $in.^3$ GI gun	1 45 + 45 $in.^3$ GI gun
Source and streamer tow depth	3 or 4 m	3 m

4. Results

Newly acquired TAMAM MCS data image structures and sediments in the upper ~1–2 km of the Marmara Sea basins in unprecedented detail. In the following sections, we describe a succession of low-stand deltas imaged in the North İmrali basin (Figs. 3 and 4), and our correlation of horizons linked to the deltas throughout Marmara Sea. Following several independent analyses, we link these low-stand deltas to specific glacial cycles, thus constructing a delta chronology. This new age model is then applied to the deformation history of the Main Marmara fault.

4.1. Low-stand delta complex

We imaged and mapped stratal geometry in the basin and intervening highs. A particular focus was a stack of delta sequences that is clearly imaged by a dense grid of MCS profiles across the southeast flank of the North İmrali Basin (Fig. 2). These data reveal a previously unknown stack of four sequences of prograding reflections with toplap characteristic of low-stand shelf edge deltas. Three of these (from top to bottom, Blue-2, "Yellow-4", and "Green-6") exhibit progradation without aggradation characteristic of "falling-stage systems tracts" (Figs. 3 and 4; Pinter et al., 2003; Piper and Aksu, 1992; Plint and Nummedal, 2000). The numbers after horizon color names represent the order of the horizon or delta complex from top to bottom. The North İmrali Basin underlies a 400 m-deep platform, and is separated from the southern continental shelf and Armutlu Peninsula by the Armutlu–İmrali fault system (also known as the Yalova fault or South Boundary fault) (Fig. 2). The WNW-striking part of this fault displays normal separation, with 200 m-high sea floor scarps. These deltas are therefore preserved due to subsidence on the downthrown side of this fault. The structure towards the middle of a major arcuate bend (concave-northward) in this border fault is manifested by a zone of progressive north tilt that absorbs most of the vertical component of deformation (the fault is mostly blind).

The stacked deltas lie between 400 m and 900 m depth on Fig. 4. The originally sub-horizontal tops of each delta are now locally progressively tilted and folded near an ENE-striking segment of the Armutlu-İmrali fault (Figs. 2 and 3). The deltas that extend sufficiently far into the basin flatten and are sub-horizontal there. Each delta consists of shingled offlapping strata dipping up to ten degrees relative to encompassing sequence boundaries. The delta terminations are sigmoidal with sharp clinoform rollovers flattening onto gentle bottomsets [Fig. 3). The deltas are capped by flat-lying strata that abruptly onlap each delta (Fig. 4). Foreset heights average 40–50 m. Thus we interpret the clinoforms to represent prodelta or depositional shelf edge deposits, which may not correspond to the shoreline . We interpret this geometry to indicate that each delta was formed within one or two tens of meters of sea level or lake level. Furthermore, we interpret the most seaward clinoform rollover to have been formed at the lowest paleo sea/lake level immediately prior to the rapid transgression that covered them.

Our interpretation of the origin of the delta is as follows. As sea level falls, the broad southern shelf becomes subaerially exposed. The subsiding North İmrali Basin became a focal point for the drainage network that developed on the exposed shelf. Presently, the Kocasu River has by far the largest drainage basin currently draining to Marmara Sea (27,600 km^2; Kazanci et al., 1999). Thus this and other rivers draining into southeast Marmara Sea during low sea levels would have bypassed the shelf and dumped sediments into North İmrali basin. However, the formation of the delta sequences requires that the water depth on the subsiding hanging-wall side of the

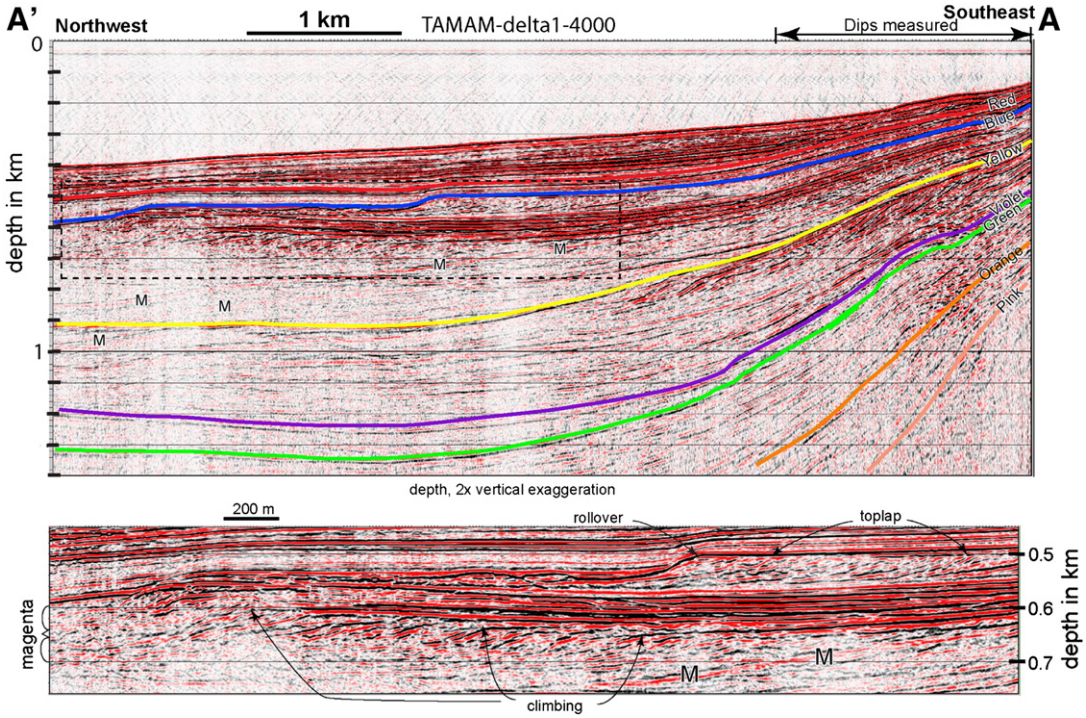

Fig. 3. Depth-migrated multichannel seismic reflection profile A–A′, displayed in depth with two times vertical exaggeration. Profile is located on Fig. 2. Color lines on top figure correspond to horizons on other figures and in text. A larger scale version of the Blue-2 delta and of the interval of a complex of deltas (Magenta-3) is shown at bottom, located by dashed rectangle (top). Magenta-3 is labeled but not represented by a colored line because it does not have a single toplap surface. Prograding strata characteristic of deltas are imaged. Apparent dips of delta tops along this profile were measured beneath the double-headed arrow. These dips are shown in Fig. 12 as "TMdelta1–4000 = e". Strata dip more steeply with depth, indicating progressive tilting. M = Multiple reflections.

Armutlu–İmrali Fault was no more than a few tens of meters. The scarp is currently about 200 m-high, too large for a sea level fall to generate deltas. In fact, above the youngest delta, we map a horizon ("Red-1"; Figs. 3 and 4) that shows mounding of sediments suggesting that sediments overflowing the shelf edge formed a lowstand wedge, but the water depth was too large for deltaic deposits (western depo-

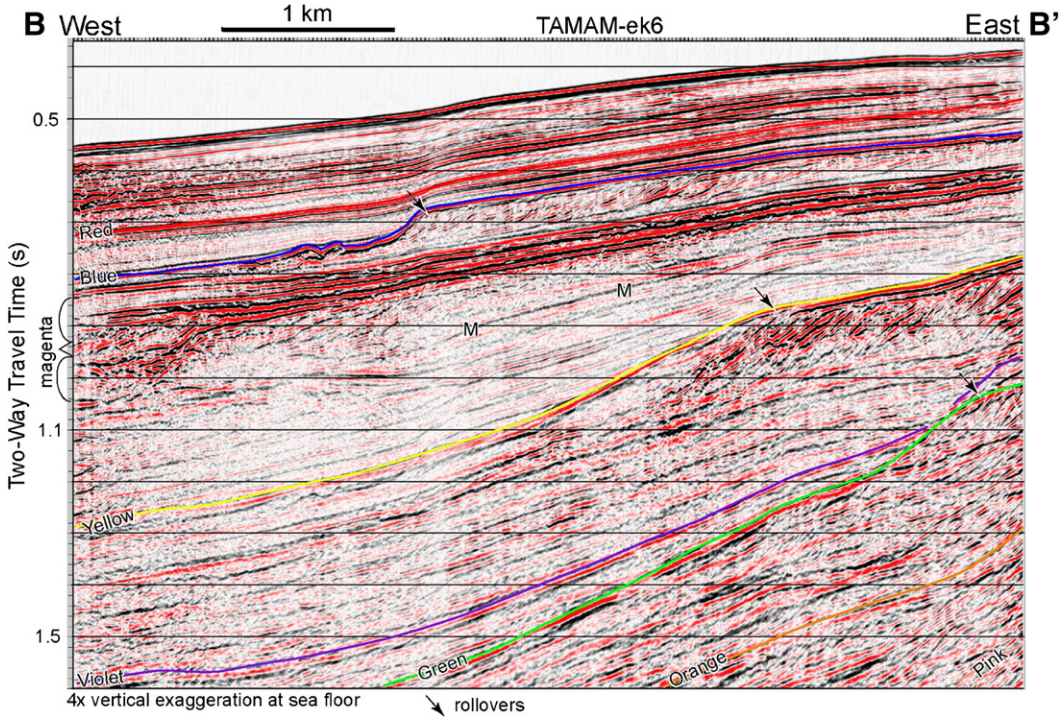

Fig. 4. Time-migrated profile B–B′, displayed in time, located on Fig. 2. Colors correspond to horizons on other figures and in text. Prograding strata characteristic of deltas are imaged. Clinoform rollovers, formed within one or two tens of meters of paleo-sea level, are indicated by arrows for Blue-2, Yellow-4, and Green-6. M = Multiple reflection.

center in Fig. 5). This suggests that the water depth in the İmrali Basin has increased, and that sedimentation has not been keeping up with subsidence since deposition of the Blue-2 delta (Figs. 3 and 4).

Isochore maps (Fig. 5) indicate that the depocenters of the delta shifted within the basin from north of İmrali Island (Green-6 to "Violet-5") to east of the island (Violet-5 to Blue-2), and back to the north (Blue-2 to sea floor). This is likely due to variations in the pathways of lowstand river systems during each glacial cycle. These diversions of the low-stand river systems may have been influenced by the growth of an anticline that now links İmrali Island to Armutlu Peninsula and also by changes in location of the deepest part of the bathymetric basin (similar to avulsions in deltas). The shift of deposition to the west after deposition of the Blue-2 delta allowed part of the sediment to be captured by a canyon in that area (Figs. 1 and 2). This contributed to the post-Blue-2 bathymetric deepening so that the shingled offlapping geometry no longer developed in North İmrali basin and only a lowstand wedge developed for younger strata.

We also note that the Marmara Sea is a small basin connected by narrow straits to the Black Sea (Bosphorus Strait) and the Aegean Sea (Dardenelles or Çanakkale Strait). When global sealevel falls below the sill depths of these two straits, the Marmara Sea becomes an isolated lake whose level could be different from the global ocean. However, faults with sea floor expression are present near the eastern entrance of Dardanelles Straight (Aksu et al., 1999; Gökaşan et al., 2010), and shorelines there are uplifting (Yaltirak et al., 2002). Therefore it is possible that paleo-sill depths during parts of late Quaternary time were different than at the Last Glacial Maximum, and a marine connection could have been maintained to the Aegean throughout the glacial cycles.

We presume that the deltas are associated with the 100 kyr glaciaoeustatic cycles. If all stages of the 100 ka glacial cycles were represented by deltas and there were not either extra deltas deposited within one cycle or missing cycles where no delta developed, we could just count deltas and match them to the global oxygen isotopic curve. However, geology is rarely that simple. For example, one additional glacial period likely occurred between depositions of two of these deltas. We have identified a high amplitude reflection that is an erosional unconformity on structural highs, which may be associated with prograding strata near western North İmrali basin (Violet-5, Figs. 3 and 4). Other horizons below Green-6, the lowest interpreted delta sequence, including "Orange-7", are associated with delta-like outlines and/or possible prograding strata in the western part of North İmrali basin. We also note that the "Magenta-3" complex of prograding strata is not a falling-stage systems tract (Figs. 3 and 4). It is just below Blue-2 and may not represent a glacial stage separate from Blue-2; Magenta-3 is further discussed in "Section 4.4" below.

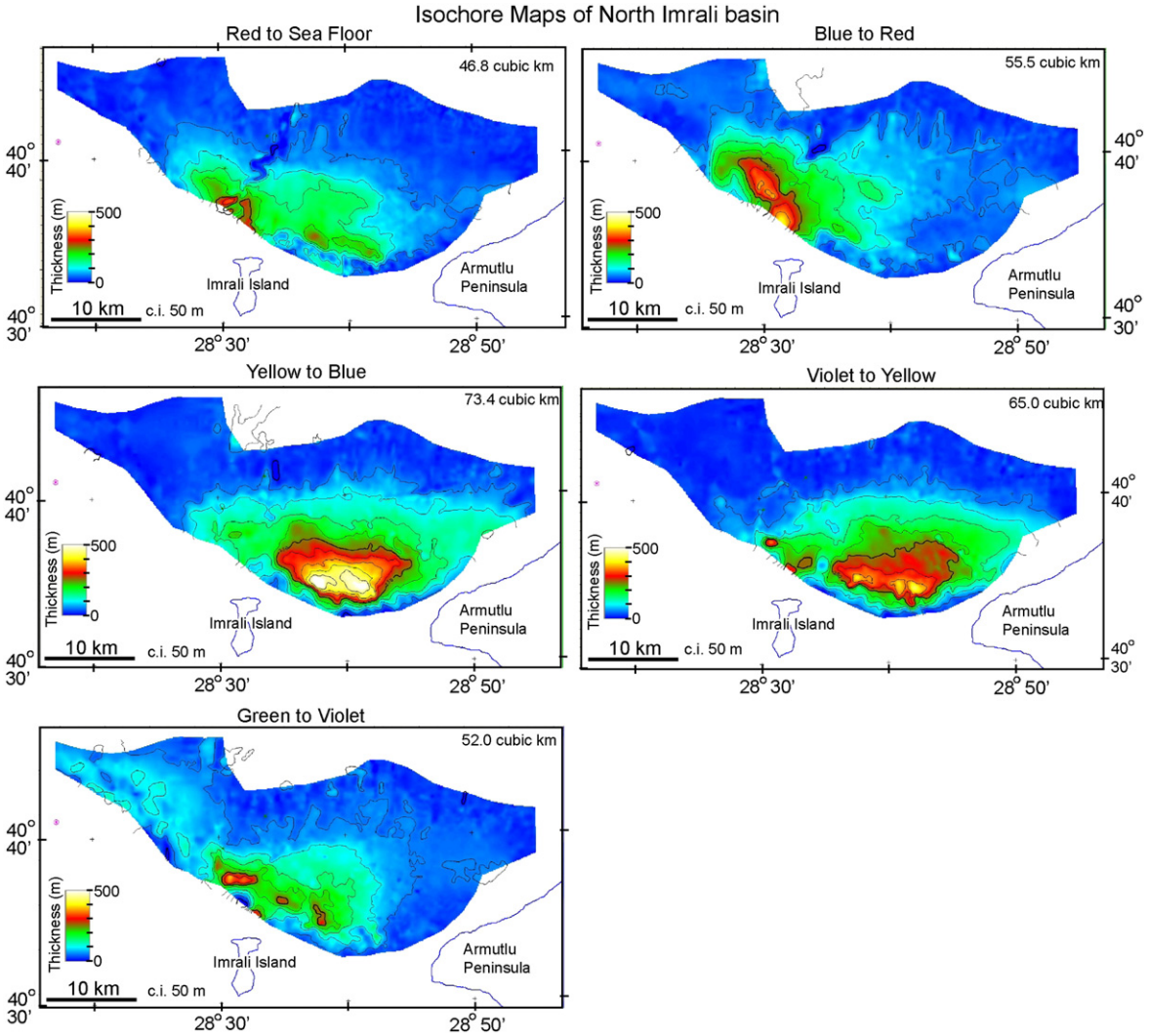

Fig. 5. Isochore maps of vertical thickness between gridded horizons. The depocenter has moved around North İmrali basin because of structural growth diverting river systems on the shelf, and likely because of changes in the location of the deepest part of the paleo-basins. These isochore grids were used for the volume calculations displayed in Fig. 9.

4.2. Mapping of the delta stratigraphy

Starting from the area of the deltas where the geometry of the sequences is clearly expressed, the toplap boundaries of each of the delta sequences were traced basinward. Standard "loop-tying" methods for 2D seismic reflection data were used to extend the correlation. The correlative conformity surfaces of the sequence boundaries corresponded to strong reflections that we were able to correlate throughout the grids of seismic reflection data (Figs. 2 and 3). The distinctive pattern of high amplitude reflections separated by transparent intervals made correlation possible across certain faults or collapse/creep folds (Shillington et al., in review; Figs. 6, 7, 8, supplemental Figs. S1, S2). TAMAM strike lines during the 2008 cruise were carefully positioned using existing data and dip profiles as they were acquired, so that they could be used for regional stratigraphic correlation. Strike lines acquired during the 2010 cruise had the advantage of fuller sequence stratigraphic analysis between the two cruises for precisely locating the lines. Correlation through the grids of intersecting profiles provided redundancy and error correction.

The horizons were mapped throughout the North İmrali Basin and correlated into the Kumburgaz Basin and the Çinarcik Basin (Figs. 6, 8, Supplemental Figure S1; Kurt et al., 2011). The horizons were also correlated into the Central Basin (Fig. 7). We have not yet been able to directly correlate the horizons to the Tekirdağ Basin in the westernmost Marmara Sea.

The mapped horizons in the North İmrali Basin were gridded and converted to depth using the following procedure: data points for each horizon were exported with a spacing of ~100 m along profiles. The program SURFACE III (Kansas Geological Survey) "Projection of Slopes", using octant search and fourth power weighting, was used to produce smooth 100 m grids for each horizon.

For conversion to depth, we used a 1D velocity model for depth below seafloor (linear velocity equation, Sheriff, 1973; Tolmachoff, 1993).

$$V(Z) = Vo + C^{*}Z, \tag{1}$$

where V(Z) is velocity below sea floor, Vo is the interval velocity at the sea floor (1514 m/s) and C is a constant whose value is 0.6. Table 2 shows a comparison of velocity estimates from Eq. (1) to independent estimates of interval velocity. The agreement is excellent except for the deepest comparison in Çinarcik Basin and the comparison using stacking velocities in North İmrali Basin. Interval velocity derived from stacking velocity is generally an overestimate of 10% (Hughes, 1985), so the 20% disagreement in Table 2 can be adjusted to 10%. The Linear Velocity Equation yields the following formula for depth conversion:

$$Z = \left(e^{C*T/2} - 1\right)*(Vo/C) \tag{2}$$

where T is the interval two-way travel time. To calculate travel time below sea floor, we converted the grid of multibeam bathymetric data (Rangin et al., 2001) to two-way travel time (TWTT) using CTD water velocity information data for the deep Marmara Sea basins (CTDs from R.V. Urania Cruise, e.g. Cormier et al., 2006, provided by M.-H. Cormier). The horizon grids were subtracted from the sea floor TWTT grid, resulting in isochron (interval TWTT) grids. The grids were then converted to vertical thickness (isochores) using Eq. (2). Water depth was added to thickness to produce depth grids (Fig. 2). Depth grids were subtracted from each other to produce interval isochore grids (Fig. 5). Volumes for each interval were calculated using "The Kingdom Suite" (Fig. 9).

4.3. Stratigraphic-age model

There are few stratigraphic age data from wells for Quaternary strata in Marmara Sea, and none for the deep basins. Hence, existing age control is limited to about 150 ka on the shelves (e.g., Çağatay et al., 2009), to post-~40 ka radiocarbon ages in the deep basins (e.g., Beck et al., 2007), The Marmara 1 petroleum test well near the edge of the southern continental shelf recovered 51 to 112 m of undifferentiated brackish Quaternary (possibly Pliocene in lower part) sediments (Figs. 1 and 2; Marathon Petroleum Turkey Limited, 1975; see also Ergun and Ozel, 1995). We correlate our sequences to the section above 127 m where we see a major unconformity. This paper, using seismic stratigraphy and the Quaternary global climate record, contains the first attempt to extend the stratigraphic age models for the basins through much of late Quaternary time (last ~800 ka). Based on this stratigraphic analysis, we are then able to examine rates and absolute timing of deformation of the transform basins in Marmara Sea.

The stack of shelf-edge delta sequences within the partly-filled North İmrali basin forms the basis for our development of an age model. The foreset/toplap geometry characteristic of these deltas could not have formed in their present position basinward of the shelf edge, even if the depth they were formed in was less than the current 300 to 400 m water depth. They must be associated with a

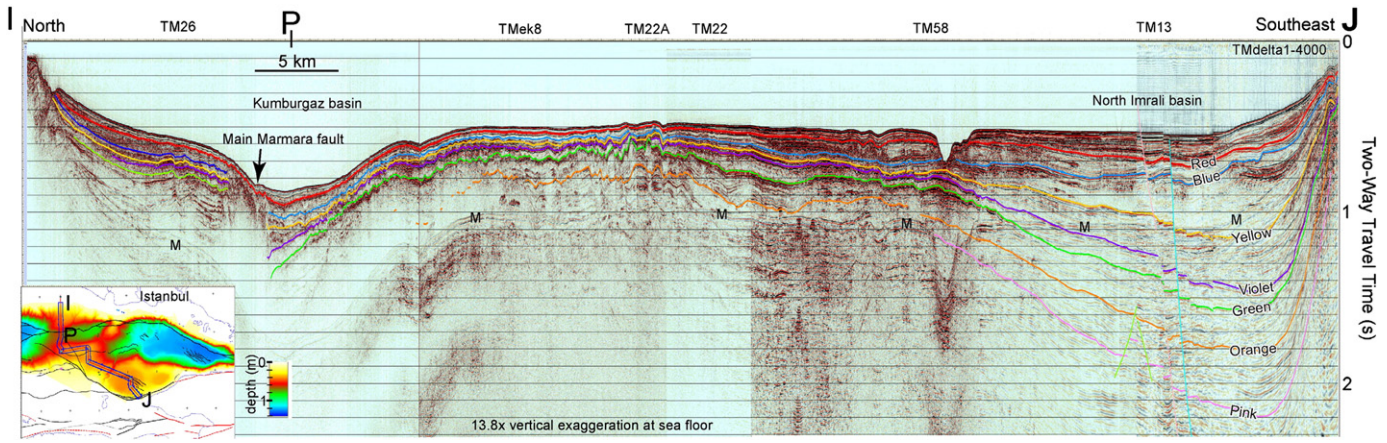

Fig. 6. Regional correlation of horizons from the area of the deltas in North İmrali basin to north of the Main Marmara fault in Kumburgaz basin. Correlation profile located on inset map by blue polygon. Fanning of dips in both Kumburgaz and North Imrali basin represents tilting. Faults and bathymetry are shown in the inset map. Colors correspond to figures and text in the paper. The stratigraphic correlation is based on all seismic reflection data in Fig. 2 and not just on this single path.

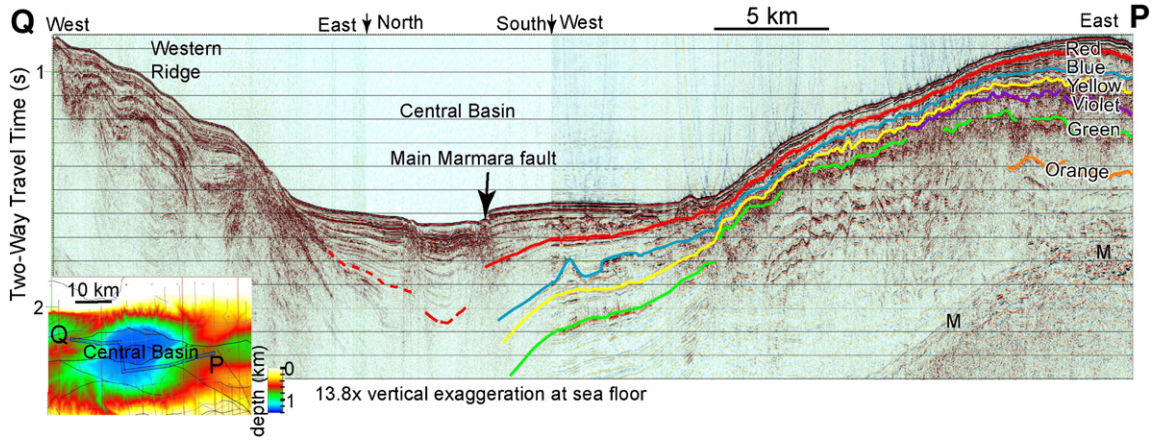

Fig. 7. Regional correlation of horizons from point "P" in the saddle between Kumburgaz Basin and Central Basin. This profile intersects Fig. 6 at point "P". It is located on inset map by blue polygon. Faults and bathymetry are shown in the inset map. Colors correspond to figures and text in the paper. The stratigraphic correlation is based on all seismic reflection data in Fig. 2 and this inset and not just on this single path.

significant sea level fall. We therefore interpret that sequence boundary capping the falling-stage systems tracts for the Blue-2, Yellow-4, and Green-6 delta sequences, each represent a glacial interval. The main question is to which glacial cycles do they correlate? Glacial intervals and sea level minima occurred approximately every 100 ka during the late Pleistocene (Lisiecki and Raymo, 2005). As a start, we make the following assumptions: 1) Marmara Sea has been connected to global oceans during each interglacial time (Beşiktepe et al., 1994); 2) the lake shoreline that formed at 87 m during the Last Glacial Maximum was controlled by the depth of a paleo-sill in the Dardanelles (Cormier et al., 2006); 3) Previous glacial Marmara lakes did not dry out more than tens of meters (if at all) below the Dardanelles paleo-sill depth; and 4) the sill depth was not greatly shallower than today over the last few hundred thousand years, and if significantly deeper than today, then global eustatic lowstands represent the minimum elevation of Marmara Sea surfaces. Together these assumptions simply mean the Marmara Sea alternated between a high level controlled by global sea level and a low sea/lake level determined by either the glacial minima or the Dardanelles sill depth.

To estimate the relative and then absolute age of the delta sequences, we use three different quantitative approaches. We initially assume relatively constant rates of structural growth and sediment deposition and subsequently relax those assumptions. These are: 1). Dips of delta horizons on progressively-tilting fold limbs at five locations, with four locations being spaced from >10 to >20 km apart; 2). Vertical part of slip ("vertical separation" or "throw") of each delta horizon across each of four NW-striking faults within North İmrali basin, assuming constant rates of vertical separation; and 3) Total corrected volumes of sedimentary rock between delta horizons for all of North İmrali basin.

4.3.1. Age of Red-1 horizon

All of these approaches provide relative ages and therefore require an estimate for the age of one horizon in order to scale the age

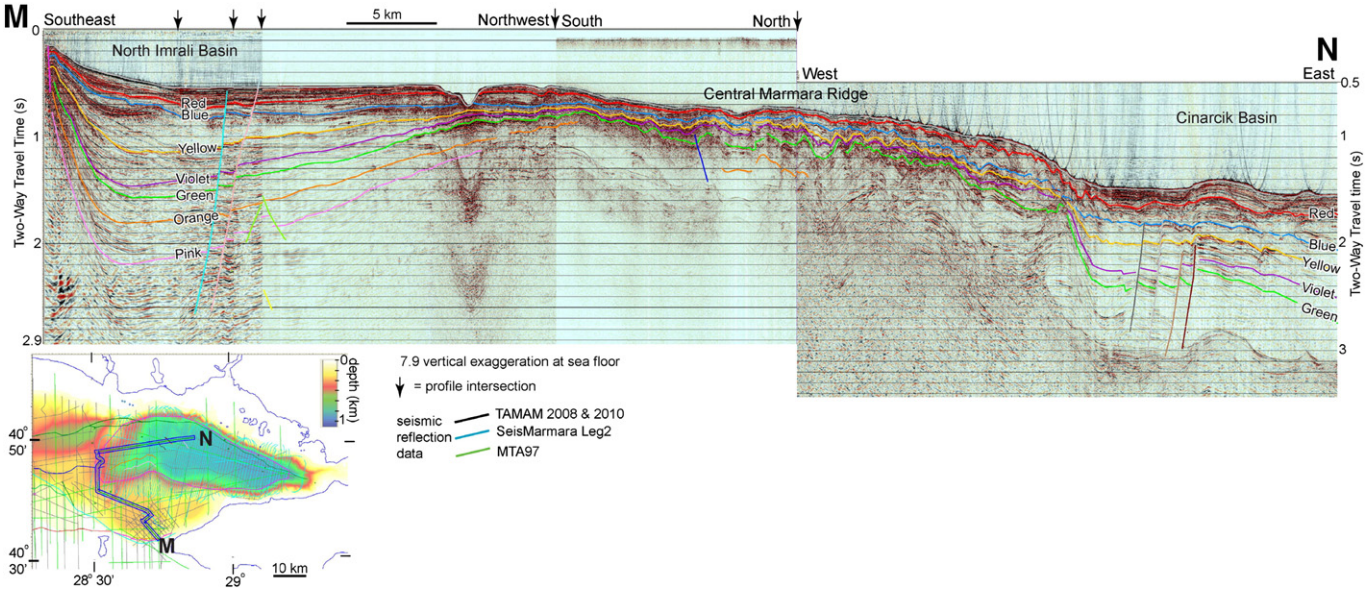

Fig. 8. Regional correlation of horizons from North İmrali Basin to western Çinarcik Basin. This multichannel seismic reflection profile is located on the inset map by blue polygon between "M" and "N". Faults and bathymetry are shown in the inset map. Colors correspond to figures and text in the paper. The stratigraphic correlation is based on all seismic reflection data in Fig. 2 and this inset and not just on this single path.

Table 2
Comparisons between use of Eq. (1) for velocity against results from refraction seismic in Central and Cinarcik basins, a checkshot velocity survey at the Marmara 1 well, and interval velocity derived from our stacking velocity analysis in North İmrali basin. "bsf" = below sea floor; TWTT = two-way travel time; SM2 = SeisMarmara Leg 2.

Location	Depth/time	Int. vel. (Eq. 1)	Comparison reference	Method	Measured velocity	
Marmara 1 well	115 m bsf	1583 m/s	Marmara 1 well	checkshot	1667 m/s	+5%
N İmrali basin	0.477 s TWTT bsf	1747 m/s	Average of 5 TAMAM profiles, 59 analyses,	Interval vel. From stack vel.	2105 m/s	+20%
Central Basin (deepest part)	1.6 s TWTT bsf	2453 m/s	Bécel et al., 2010 OBS profile SM03	Refraction	2500 m/s	+2%
SM2 Line 134	2336 m bsf	2920 m/s	Dessa et al., 2007	Refraction	3400 m/s	+16%

estimates for the other horizons. We therefore first estimate the age of the youngest interpreted horizon, Red-1. Red-1 has not been correlated to an imaged delta, but is a high-amplitude reflection compatible with a sandy interval, and it is locally an unconformity. A giant piston core collected with the R/V *Marion Dufresne*, MD01-2431, in the southern Central Basin (Fig. 1) has a radiocarbon date of 16.3 to 17.4 ka at 17 m below sea floor (bsf) (Beck et al., 2007). The Red-1 horizon close to that core is about 110 m bsf. Extrapolating 17 ka at 17 m bsf provides an estimate of 110 ka for the Red-1 horizon.

An immediate question raised is whether Red-1 could correspond to Oxygen Isotope Stage (OIS) 6 at 140 ka? To address this we examine the stratigraphy associated with Red-1. Seeber et al (2006) proposed a sedimentation-age model for the Marmara Sea that incorporates variable sediment supply in a constantly tilting tectonic basin. They propose low sedimentation rates in basins during transgressions and highstands of sea level when sediment is stored on the inner shelves. In contrast, during regressions, shelf sediments are reworked and increase the sediment supply to offshore basins. The result is that slow interglacial sedimentation over a longer time produces strata that show greater fanning of dips in profile than the same thickness of rapidly deposited glacial-period sediment. Seeber et al. (2006) demonstrate an over five fold increase in fanning above the 14 ka lake-sea transition in the Çinarcik Basin. Our seismic data image prominent differentially tilted units in each of three basins. Fig. 10 illustrates two wedges of onlapping reflections with fanning of dips in the Central Basin that we correlate to OIS 5 and OIS 7. The upper wedge in the Central Basin and in the other basins are interpreted as being transgressive and high-stand deposits from Oxygen Isotopic Stage (OIS) 5e at about 125 ka. In all three basins, the upper progressively tilted units occur just below Red-1. We therefore conclude that Red-1 is younger than the OIS 6 (140 ka) and was deposited in the minor low-stand at 109 ka (Lisiecki and Raymo, 2005). This age estimate for Red-1 is very close to the extrapolations below the piston core MD01-2431. The estimate can be tested: Core MD04-2743 reached or almost reached Red-1, but unfortunately, the deeper parts of this core have not yet been dated (located on Fig. 1).

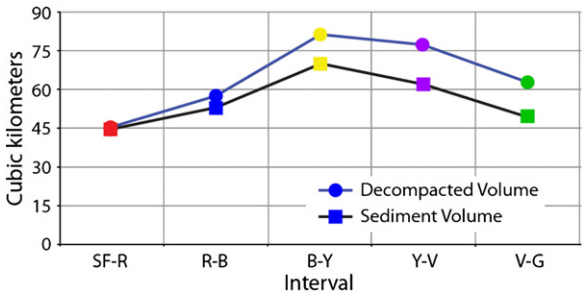

Fig. 9. Volumes for intervals between interpreted stratigraphic horizons for all of North İmrali basin (triangles). The area where volumes are measured is outlined on Figs. 2 and 5. Colors correspond to the base of each interval. SF = Sea Floor; R = Red-1; B = Blue-2; Y = Yellow-4; V = Violet-5; G = Green-6. Squares give corrected, decompacted volumes, as described in text. If Red-1 is 109 ka, and the rate of sediment accumulation is constant, then Blue-2 is 243 ka, using corrected volumes. We assume that Blue-2, Yellow-4, and Green-6, which correlate to deltas, were deposited during relatively falling sea levels and are assigned the age of the most positive value of the Oxygen Isotopic curve of Lisiecki and Raymo (2005).

4.3.2. Relative ages from progressive tilting

In order to obtain relative ages of other reflectors, we examine the dips of seven horizons, including the sea floor, as measured on depth-migrated seismic reflection profiles at five locations (labeled "a" through "e" on Fig. 2). Two of these profiles are displayed in Figs. 3 and 11. Dips are plotted on Fig. 12. We assume a relatively flat-lying surface has been progressively tilted and that the preserved strata record this rotation. The main limitations with this approach is that for some sites, sea floor dip is non-zero, meaning that not all of the tilting has been filled by sedimentation, and consequently we do not know if the initial dips were zero. We therefore consider the sites where the surface dip is close to zero as the most reliable. In order to calculate the progressive tilt, the dip at the sea floor was subtracted from the dip of each horizon. The linearity of the increasing dips suggests relative equal time spacing between horizons and thus representation of each ~100 ky glacial cycle.

4.3.3. Relative ages from vertical separation of horizons at faults

The second approach for obtaining relative ages involves the vertical separation across the set of NW-striking extensional or transtensional faults within North İmrali basin (Fig. 13). Assuming continuous growth should yield linearly increasing vertical separation. Separation for each horizon was measured in two-way travel time at 23 locations total for the four faults where all these horizons could be unequivocally identified (Fig. 14). Travel time was converted to depth using Eq. (2). Limitations of this method are when faulting exceeds the rate of sedimentation, some of the throw contributes to scarp development rather than differential sedimentation. Scarp height was measured at each location. The most reliable estimates are considered sites with little to no surface scarp.

Overall, the plot shows continuous growth in vertical separation with the following observations. Flat slopes on the graph suggest that faults "c" and "d", and part of "b" did not start slipping at their full rate until after Violet-5. Similarly, fault "a" was mainly active after Yellow-4 time. An alternate explanation would be that the time interval between Violet-5 and Green-6 is shorter than the other intervals.

4.3.4. Relative ages from sediment volumes

For the third method, we use sedimentary volumes for the entire North İmrali basin between interpreted horizons and the assumption of steady sediment input to the basin per glacial cycle. We used the gridded horizons to estimate sediment volumes (Figs. 5 and 9). To correct for compaction of the sediments at depth, we make use of the velocity model used for depth conversion. We convert from velocity (vs. depth) to density using Eq. (1) from Brocher (2005) and then from density to porosity by assuming a grain density of 2680 kg/m^3. The resulting porosity-depth curve is well fit by an exponential decrease in porosity with depth down to 1800 m, the maximum depth of the Green-6 horizon surface in North İmrali Basin (Fig. 2). The resulting equation for porosity is:

$$\Phi = 0.626^{*} e^{-0.000351Z}. \quad (3)$$

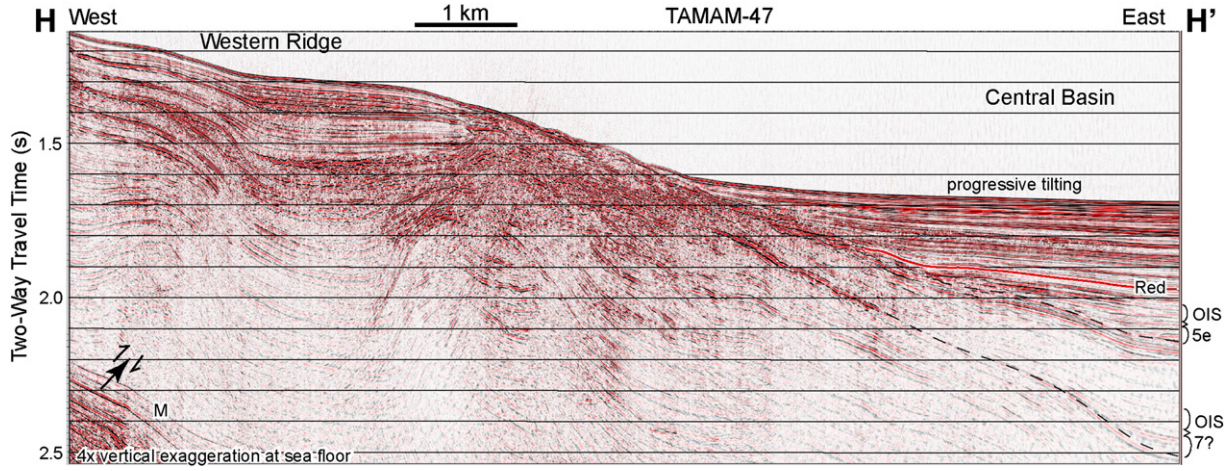

Fig.10. Migrated profile across the western margin of Central Basin located on Fig. 1. The arrows at lower left indicate the upper part of a blind thrust fault, barely imaged but supported by fold geometry. The ~100 ka (assigned 109 ka) Red-1 horizon is involved in progressive tilting (dips steeper with depth). Dashed horizons are bathyal onlap surfaces that form the bases of sedimentary wedges proposed to be deposited during interglacial times of low sedimentation rates (see Seeber et al., 2006). OIS = Oxygen isotopic stage; M = Multiple reflection. This young contractional folding on Western Ridge is only present north of the Main Marmara fault. Thus, the western margin of Central basin is not a pre-existing structure that can be used to reconstruct Central basin.

Using this equation, we estimated the decompacted volume of sediments, i.e., the thickness of sediments if they were restored to the surface porosity of 62.6%.

Fig. 9 presents the computed sediment volumes and the volumes corrected for compaction. The volumes vary by up to 29% from the mean. This is a significant amount but less than the factor of 2 expected for missed glacial cycles. The pattern shows an interval volume increase between the deposition of Violet-5 and Blue-2, and then a sharper decrease after deposition of Blue-2. The lower volumes correspond to the times when the delta depocenters are in the west (Fig. 5). In this region there is currently a canyon, visible in the isochores (Fig. 5) and the current bathymetry (Fig. 1), that bypasses sediment from the North İmrali Basin to the Çinarcik Basin. The decompacted volumes suggest that about 30% of the sediment is bypassed to the Çinarcik Basin.

4.3.5. Absolute age assignment

Using the age assignment for Red-1 as 109 ka, we can use the sediment volumes to extrapolate the age for Blue-2, as both sets of volumes are similarly affected by the canyon. Scaling the decompacted sediment volume between Blue-2 and Red-1 to that between Red-1 and Seafloor, with Red-1 assumed to be 109 ka, results in an estimate of 246 ka for Blue-2 (star in lower part of Fig. 15a). Blue-2 is therefore assigned to OIS-8 at 252 ka.

We use Blue-2 at 252 ka as the basis for extrapolating the older horizons in order to minimize the errors inherent in extrapolation. Extrapolating the ages of the older sequences based on volume relative to Blue-2 should overestimate the age because of the sediment lost from the North İmrali Basin. In fact, the decrease in sedimentation volume between the Yellow-4 and Blue-2 deltas is even more notable if the Blue-2 to Red-1 interval elapsed time interval is 143 ka and the earlier time intervals are closer to the 100 ka glacial cyclicity. Thus the stars in the upper part of Fig. 15a are an upper limit for the ages of Yellow-4, Violet-5 and Green-6. We now turn to the dips and vertical separations across faults, scaled to the age estimate for Blue-2. The vertical separations had the sea floor scarp height, if any, subtracted from the offsets at each location. The results are plotted on the upper part of Fig. 15a. The values show considerable scatter, as expected, but are centered at values lower than the volume extrapolations. Based on the extrapolations and the evidence that the

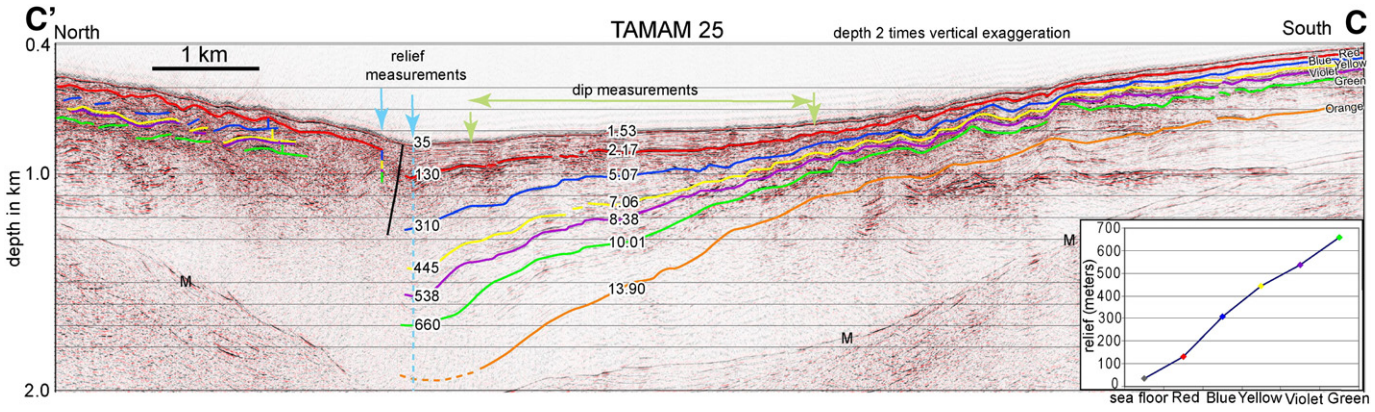

Fig. 11. Migrated depth section C–C′ displayed with two times vertical exaggeration, located on Fig. 2. Colored horizons correspond to other figures and the text. Numbers are structural relief in meters across and close to the northern strand of the North Anatolian fault, and dip in degrees. These dips suggest ongoing tilting of the basin margin since at least the time of deposition of "orange". The graph gives structural relief across the Main Marmara fault as measured at the labeled arrows. The near constant rate of relief growth between horizons, assuming near constant age interval between horizons, is consistent with uniform right-reverse slip on the Main Marmara fault through this restraining segment. These dips are shown as TM25 = a in Fig. 12. M = Multiple reflection.

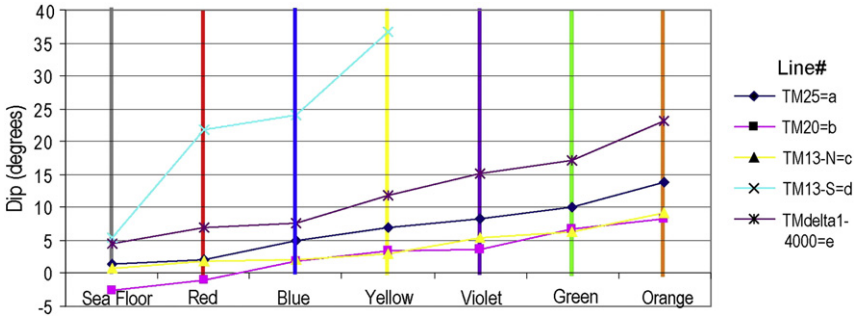

Fig. 12. Horizon dips measured on migrated depth sections at locations labeled on Fig. 2 as "a" through "e". TM25 is shown on Fig. 11; TMdelta1–4000 is seen on Fig. 3.

sequences record a complete set of 100 ky cycles with no missing or extra sequences, we assign Yellow-4 to OIS 10 (341 ky), Violet-5 to OIS 12 (434 ky) and Green-6 to OIS 14 (540 ky). We cannot rule out older ages for Yellow-4 and older horizons. Fig. 15b summarizes the age estimates and our assessment of their uncertainty as indicated by the horizontal bars.

4.4. Discussion of age model

The tilt, fault separation, and volume analyses discussed above can be used to test whether any glacial periods are not represented by a delta sequence and might be missed, or whether any delta sequences do not represent a glacial maximum on the 100 ka late Quaternary cycle. For example, if we look at the prominent deltas on the profile depicted in Fig. 3, the uncorrected and decompacted volumes between Green-6 and Yellow-4 (111/140 km^3) is much greater than the volume between Yellow-4 and Blue-2 (69/81 km^3). This suggests an extra climate cycle between Yellow-4 and Green-6 (Fig. 9). The intervening Violet-5 is not a major delta as its depocenter is farther west (Fig. 5), and it also correlates to an erosional unconformity at the crest of the current and paleo-ridge between North İmrali Basin and Çinarcik basin. The inset to Fig. 16 images sharp erosion of the Blue-2, Yellow-4, and Violet-5 horizons into the strata beneath. The pattern of pre-Blue-2 tilting compared to current depths of delta rollover (Figs. 3 and 4), supports the idea that the paleo-ridge could have been exposed to erosion at low-stand sea/lake levels. Thus, we concluded that Violet-5 also represents a glacial cycle and included it as such in our analyses.

Below the Blue-2 delta is another prograding delta complex, Magenta-3 (labeled but not colored on Figs. 3 and 4). However, the rates of tilting, fault growth and deposition between Yellow-4 and Blue-2 are similar to other intervals. If Magenta represents a separate glacial maximum distinct from Blue-2, then the sedimentation rate after deposition of Yellow-4 would be just over half the rate between Violet-5 and Yellow-4. The dip-slip rate on some of the faults (Fig. 14) would similarly decrease after deposition of Yellow-4.

Furthermore, unlike the other deltas, Magenta-3 aggrades as it progrades towards the basin (Figs. 3 and 4). The Blue-2, Yellow-4, and probably the Green-6 sequences are falling-stage system tracts with little or no aggradation during progradation. This indicates Magenta-3 was deposited during relative sea level rise, perhaps due to subsidence that was faster than the eustatic sea level fall. If global sea level dropped below the Dardanelles paleo-sill, the Marmara Sea would become a paleo-lake as it was during the last glacial. At the low lake level (the lake level at the end of the latest Pleistocene was −87 m; Cormier et al., 2006; McHugh et al., 2008), the shelves remained exposed and the sediment supply to the shelf edge delta continued. Continuing subsidence creating accommodation space with a constant lake level would have resulted in a relative lake level rise at the delta, explaining the aggradation seen at Magenta-3. Alternatively, Magenta-3 could have formed during a stillstand or slow rise of sea level during a time of overall low sea level. For example, the Magenta-3 interval may correspond with the local δO18 peak (cold and/or larger ice volume) at 292 ka and the global eustatic rise afterwards. Another possibility is Magenta-3 corresponds to OIS 8 and Blue-2 corresponds to the low sea level at OIS 7b at 223 ka. In either case, the data suggests that the Blue-2-Magenta-3 interval is not a complete glacial cycle, but due to the more complex sea level history associated with OIS 8.

In contrast, the offlap during deposition of the Blue-2, Yellow-4, and Green-6 deltas indicating relative falls in sea level suggest that sea level fall was not limited by the development of paleo-lakes in the Marmara basin at those times. Global eustatic sea level minima during late Quaternary glacial stages ranged from 86 m to 124 m below present (Miller et al., 2005). Faults near the eastern mouth of Dardanelles Straight deform the sea floor (Aksu et al., 1999; Gökaşan

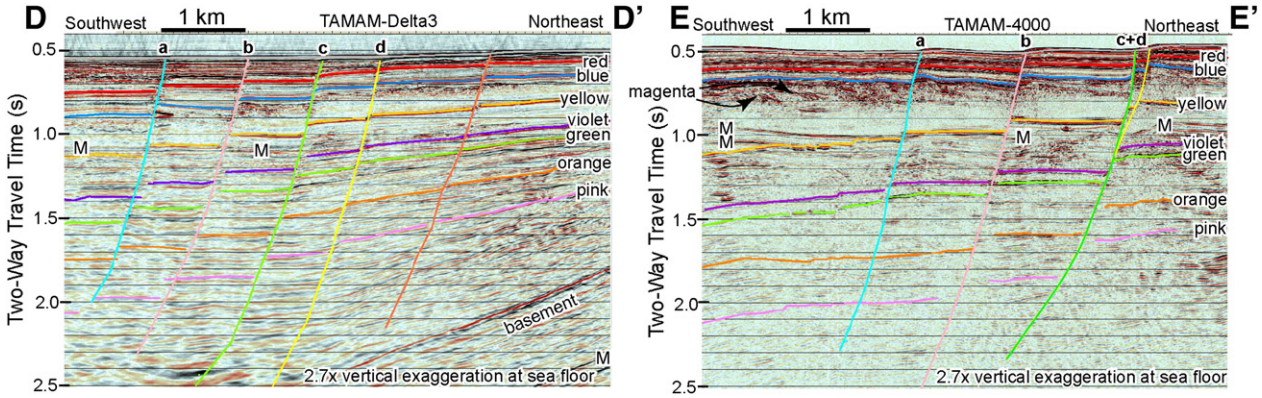

Fig. 13. Two interpreted migrated profiles located on Fig. 2. The vertical separations ("throws" of the sea floor and each horizon are measured in two-way travel time across each of faults "a" through "d", and converted to depths. These throws are plotted on Fig. 14.

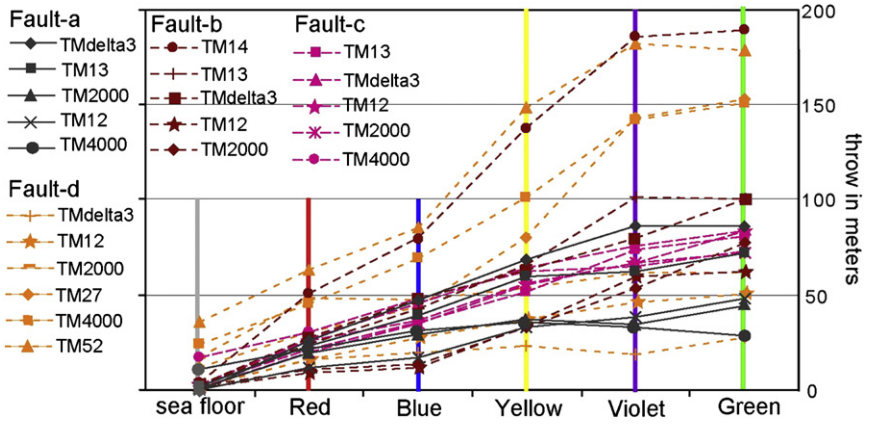

Fig. 14. Throws across faults "a" through "d" plotted at 21 locations within North İmrali basin. Colors and line pattern are distinct for each fault. If time intervals between horizons are constant, and fault throw rate is constant, the lines should be straight. Flat slopes on the graph suggest that faults "c" and "d", and part of "b" did not start slipping at full rate until after Violet-5 time and fault "a" was mainly active after Yellow-4 time.

et al., 2010), and late Quaternary marine terraces indicate uplift in this area (Yaltirak et al., 2002). Thus, the paleo-Dardanelles sill may have varied through time and have been deeper than low-stand sea levels during deposition of the Blue-2, Yellow-4, and Green-6 deltas.

As noted above, the paleowater depth at Red-1 was too great for a delta to be formed. Red-1 corresponds to a lowstand wedge. This deepening after formation of the Blue-2 delta is likely influenced by the capture of sediment by the canyon; decreased sediment input into North İmrali basin would result in subsidence out-pacing subsidence. Thus the resulting deepening of the North İmrali Basin from to lowered sediment input would have prevented the formation of younger deltas. In fact, the present-day 400 m depth of the North İmrali Basin and 250 m drop at the edge of the Southern Shelf prevented a delta from forming there during the last glacial stage, OIS-2.

If Blue-2 corresponds to OIS-8, and Red-1 post-dates OIS-5, then the penultimate glacial interval, OIS-6, is not represented in our

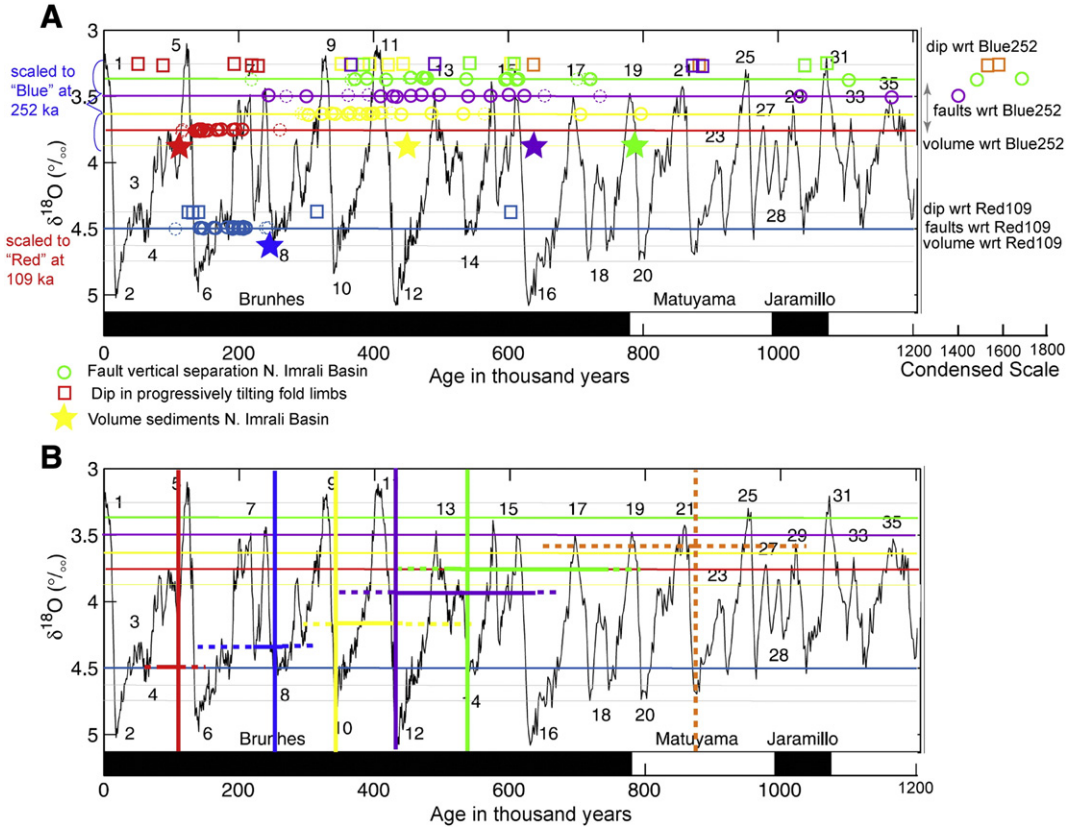

Fig. 15. A: Data points for age with respect to Red-1 (bottom) or with respect to (wrt) Blue-2 (top) plotted on the oxygen isotopic stage (OIS) record of Lisiecki and Raymo (2005). The lower part of plot shows calculated ages for Blue-2 calculated with respect to an age for Red-1 of 109 ka. These are for sedimentary volume (star), throw across faults (circles), and dip (squares). Volume is relied on to assign Blue-2 to OIS 8 at 252 ka; fault throw and limb dips are both permissive of either OIS6 or OIS 8. The upper part of plot gives calculated ages for the other horizons with respect to Blue-2 at Oxygen Isotopic Stage 8 at 252 ka. Thin dashed circles are those data points for fault throw with sea floor scarps exceeding 10 m. High values (down) on the oxygen isotopic curve represent glacial intervals, given even numbers (2, 6, 8…). Ages are 140, 252, 341, 433, 536, 630, 718, and 794 ka for OIS 6 through 20 evens. B: Preferred age model given by vertical color bars. Solid horizontal bars represent likely range, and dashed horizontal bars represent plausible range. Ranges qualitatively estimated from data points in the Figure.

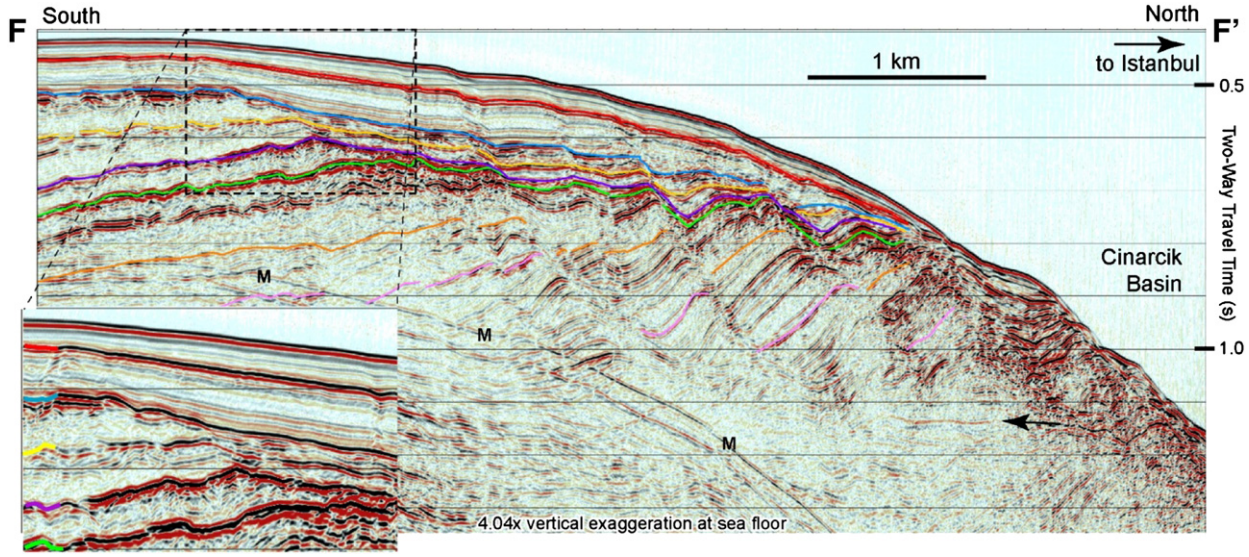

Fig. 16. Migrated profile F–F′, located on Fig. 2. Top is 0.4 s two-way travel time, not sea surface. Red-1 and Green-6 erode strata beneath. The inset shows erosion of the Blue-2, Yellow-4, and Violet-5 horizons into the strata beneath. The erosion at Violet-5 time supports assigning it to a glacial interval. Low-angle listric normal faults root above unfaulted strata (arrow), and accomplish a gravitational collapse into ÇinarcikBasin. The Orange-7 horizon is about 800 ka or older (Fig. 15). Part of the >1.1 km on the basal fault occurred before deposition of Orange-7. "M"s are multiple reflections.

delta horizons. We do note that unconformities and strong reflections are present between Blue-2 and Red-1, especially near the depocenter for this interval (Fig. 5) north of İmrali Island, but were not mapped. It is also possible that a delta corresponding to OIS-6, or the sea level fall leading up to it, is one of those imaged on the southern shelf northwest of İmrali Island by high-resolution sparker seismic reflection data (Figs. 12 and 13 in Aksu et al., 1999).

The pattern of fault throw across the series of seismic horizons (Fig. 14) shows an approximately smooth increases in throw starting at Yellow-4 time. However, the Green-6 and Violet-5 horizons have about the same vertical offset across faults. This could be taken to suggest that there is little age difference between the 2 horizons. However, the sediment volumes and tilt rates suggest otherwise. Thus we suggest that faults "c", "d", and part of "b" were not active at high rates until after Violet-5 was deposited. Since these faults were not very active until after Violet-5 time, throw on these faults provides no information on the relative age of Green-6.

5. Discussion

The development of a stratigraphic framework and tentative age model enables evaluation of tectonic models proposed for the Marmara Sea. Any choice of age model within the "plausible" range of Fig. 15B, combined with the regional correlation of the stratigraphic horizons between basins (Figs. 6, 7, 8; Supplemental Figs. S1, S2), allows the "steady state" vs. "young reorganization models" to be tested. The correlated stratigraphy and age model are also able to document the slow continuous collapse of the southern margin of Çinarcik Basin (Shillington et al., in review).

Regional correlations of our stratigraphic model indicate that slow downslope motions have occurred for at least 500 ka over large parts of Marmara Sea (Shillington et al., in review).

The widespread occurrence of these features suggests that downslope failure is an important mechanism for sediment transport into the basins. The listric normal faults are present only in the upper few hundred meters of the sub-bottom and are therefore not expected to be seismogenic. These progressive gravitational collapses are also not catastrophic submarine landslides, and thus would not trigger landslide-generated tsunamis. However, they can provide important clues to the temporal and spatial development of basins through time since they should respond to changes in sea floor slope and tilt. For example, seismic reflection profiles image a family of listric normal faults at the escarpment between North İmrali and Çinarcik basins (Fig. 16).They are similar in form to faults imaged in the Gulf of Mexico (e.g., Winker and Edwards, 1983), but of much smaller dimensions. The distinct reflection pattern enabled us to correlate across these faults. We found that the most active interval of normal slip is younger on the more basinward faults suggesting a migration of fault activity. The faults appear to sole onto a sub-horizontal basal-decollement (arrow in Fig. 16). The horizontal separation (heave) of the lowermost correlated horizon ("Pink-8") totals 1.1 km on the 3 southern strands, so slip on decollement (arrow in Fig. 16) must exceed that amount. While we have not extended our age model below Green-6, tilting and counting sequences suggest that the age of the Orange-7 horizon exceeds 800 ka (Figs. 11, 15) The gravitational collapse into the Çinarcik basin initiated well before Orange-7, thus the interpretations for initiation of the Marmara Sea basins and of slip on the Main Marmara fault at ~1400 ka (Seeber et al., 2004) or 1700–2000 ka for Çinarcik basin (Carton et al., 2007) are compatible with our observations.

The reflections corresponding to the deltas have been correlated across a large fraction of Marmara Sea, including much of Kumburgaz basin (Figs. 6, 7, 11, Supplemental Fig. S2) and all of Çinarcik basin (Fig. 8; Supplemental Fig. S1; Kurt et al., 2011). The stratigraphy thus enables us to examine the temporal history of the tectonics in these regions. In western Kumburgaz basin, the Red-1 horizon can be directly traced across the northern strand of the NAF, The delta horizons below, through Green-6, can be correlated across the fault through a close pattern match on several profiles in Kumburgaz basin (Supplemental Fig. S2). All of these horizons exhibit steeper dip with increasing depth along the progressively-tilting southern margin of Kumburgaz basin (Fig. 11). Similar to İmren et al., 2001 and Demirbağ et al, 2003, we interpret a reverse component of slip across the shallow N-dipping part of the Main Marmara Fault. Thus, we ascribe the Kumburgaz Basin to a restraining segment (Figs. 1, 2 and 17) in contrast with the transtensional origin of the three deepest bathymetric basins in Marmara Sea (Armijo et al., 2002; Seeber et al., 2004, 2006; Okay et al., 2004). Using the cross-fault correlations, we estimated the vertical component of slip across the Main Marmara fault, assuming that the current seafloor slope and offset across the

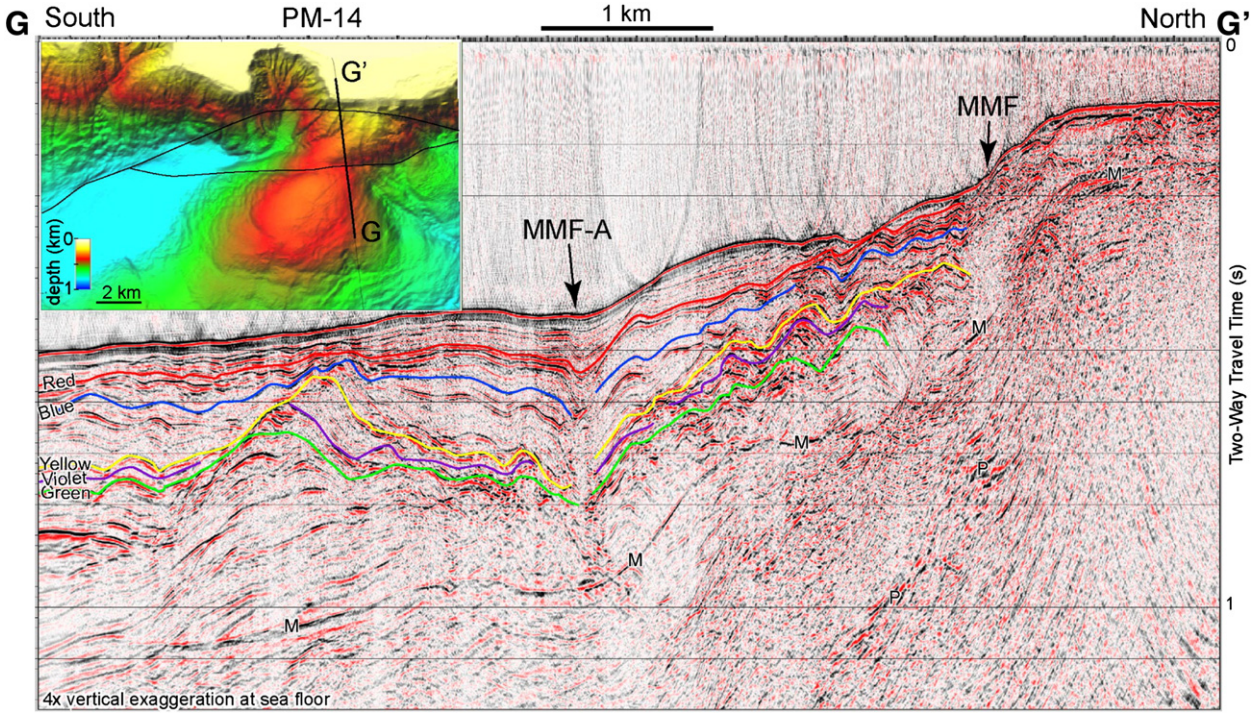

Fig. 17. Migrated profile collected in 2010 across Central Marmara Ridge, located on inset and Fig. 2; the inset map is located on Fig. 2 as the black dashed rectangle. The inset is a shaded-relief display of a 20 m grid of multibeam bathymetry from Rangin et al. (2001). MMF-A is the Main Marmara fault of Armijo et al. (2002) responsible for a 3.5 km right-lateral offset of the NNE–SSW Central Marmara Ridge. Stratigraphy is correlated across this fault (less reliably for Green-6, and not reliably for Violet-5). The northern, "MMF" strand presumably carries additional right-lateral slip. M = Multiple reflection; P = Primary reflection (likely from basement).

fault has remained roughly similar through time (Fig. 11 inset). While the tilt rate in the Kumburgaz Basin need not be constant, there is no evidence for any abrupt change in deformation. In fact, using the age model, the dip-slip rate vs. time is even more linear than the dip-slip vs. horizon color inset in Fig. 11. We conclude that there has been relatively uniform slip through time without any evidence of a major reorganization of active fault strands, leading to a uniform rate of growth of structural relief across this restraining segment of the Main Marmara fault, (Fig. 11 inset).

Thus the Kumburgaz and North İmrali Basin, as well as the other basins where we have interpreted the stratigraphy exhibit "steady state" basin growth with no evidence of a sharp change in the last >500 ka. Our "steady-state" model challenges several published reconstructions along the Main Marmara fault that interpret a "young reorganization". For example, Armijo et al (2002) interpret right offset of the Central Marmara Ridge of 3.5 km, and calculate that this offset would accumulate in 140 to 350 ky for slip rates of 1 to 2.5 cm/yr. This offset has been used by others to propose that the Main Marmara Fault did not initiate until 200 ± 100 ka (Demirbağ et al., 2003; İmren et al., 2001; Le Pichon et al., 2003; Rangin et al., 2004; Sengör et al., 2005). Alternatively, we interpret that the Main Marmara fault splits into two strands across Central Marmara Ridge, and that the obvious morphologic offset noted by Armijo et al. (2002) is due to slip on the southern strand (MMF-A in Fig. 17). If the southern strand now carries most of the slip, then it may have initiated when proposed by these authors. However, when this strand initiated may have limited significance because the two strands merge together both in Kumburgaz Basin to the west and Çinarcik basin to the east of Central Marmara Ridge (Figs. 1, 2 and 17). Much larger total displacements may be carried on the northern strand. Thus, the offset of Central Marmara Ridge by MMF-A places no constraints on when the current large-scale geometry and kinematics of the Main Marmara fault initiated

Estimates for 4 km of total right-lateral displacement on the Main Marmara fault are also based on restoration of Central Basin to a parallelogram shape (Le Pichon et al., 2003). However, asymmetric basins may form due to oblique slip on Main Marmara fault strands (Seeber et al, 2004, 2010). The Western Ridge that bounds the west side of Central Basin north of the Main Marmara fault is a series of young contractional folds (Fig. 10; İmren et al., 2001; Rangin et al, 2004) and thus not an older offset structure. Right-lateral slip is also likely accommodated on a fault along the northern margin of Central Basin, which we hypothesize drives the contraction of Western Ridge via a >5 km restraining left stepover (Fig. 1).

Another argument for young reorganization of structure of Marmara Sea (at about 200 ± 100 ka) is based on abandonment of faults, assumed to be normal faults, at the margins of the basins and focusing of deformation on the Main Marmara Fault (İmren et al., 2001; Rangin et al., 2004). One of these presumed abandoned faults is the İmrali fault bounding North İmrali basin (İmren et al., 2001). However, the İmrali fault has several strands and only one of these strands may be buried beneath younger sediments. Thus we see no evidence for a cessation of activity of this fault. Farther west, faults bounding the Central basin may also still be active. The northern fault has a sea floor scarp "x" in Fig. 1), and the southern fault also deforms the sea floor, although we interpret part of the bathymetric scarp to be the result of onlapping strata, not faulting ("y" in Fig. 1). There is also a fault system along the shelf break south of Central basin, but it is involved with and obscured by gravitational collapses including a family of listric normal faults. We thus see little evidence for late Quaternary abandonment of extensional faults.

Sengör et al. (2005) proposed an evolutionary model that has the NAF evolving from a broad zone of the various types of Riedel shears and folds, as seen in analog models (e.g., Wilcox et al., 1973), towards a single discrete fault. He further proposes that this transition has been propagating westward since the Middle Miocene finally reaching the

Marmara Sea region about 200 ka. Thus in the early stage, the plate displacement in the Marmara region was accommodated by multiple oblique faults and substantial displacement was accommodated before it was superceded by a single discrete fault. However, seismic reflection data present no evidence for structures different from those active today which are capable of having absorbed several tens of km of block motion. These classic analog models may be inappropriate for a fault system known to be reactivating pre-existing structure such as the Intra-Pontide suture (Seeber et al., 2004; Sengör et al., 1985). There is no strong evidence for change in basin formation and fault slip for at least the last 536 ka in North İmrali and Kumburgaz basins. This is consistent with the interpretation that the vertical separation of strata across the Main Marmara fault through Central basin increases with age throughout filling of that basin (Laigle et al., 2008). The evidence supports a model where most extension is due to oblique right-normal slip on a non-vertical NAF through releasing segments associated with Tekirdağ and Çinarcik basins (Okay et al., 2004; Seeber et al., 2004, 2006).

6. Conclusions

We present new high-resolution multichannel seismic data that enable the development of the first detailed stratigraphic model for the Marmara Sea basins below the depths of existing piston cores. The discovery of a suite of lowstand deltas in the North İmrali Basin allowed the development of an age model for the stratigraphy back to >500 ka. Regional correlations of stratigraphic horizons along the Main Marmara Fault and basin margins supports steady-state deformation during this time.

Supplementary materials related to this article can be found online at doi:10.1016/j.tecto.2011.10.006.

Acknowledgments

We thank the captains and crews of the R/V Piri Reis for the 2008 TAMAM cruise and the short but critical 2010 PirMarmara leg a4 cruise. Additional members of the TAMAM 2008 scientific party are Evren Buyukasik, Melis Cevatoglu, Suleyman Coskun, and Pinar Özer, who processed F–F′ shown in Fugure 16. Emin Demirbağ organized the I.T.U. effort. Additional members of the PirMarmara 2010 scientific party include Orhan Atgin, Özkan Özel, Hakan Saritas, Jean Charles Guedes and Yannick Thomas; Guedes and Thomas were critical to the data acquisition. Organizers of a 2006 workshop in Istanbul important to our international collaboration included Naci Görür, Cenk Yaltirak, Gulsen Ucarkus, Marie-Helene Cormier, and others. Cecilia McHugh contributed stratigraphic discussions. Refraction interpretations were made available by Jean-Xavier Dessa; Satish Singh, Helene Carton, and Pierre Henry provided seismic reflection and bathymetry data on websites. Marie-Helene Cormier provided a comprehensive edit. Editor Fabrizio Storti and an anonymous reviewer provided constructive comments. We thank Hydroscience Technologies, Inc. for their valuable support for the seismic systems of Piri Reis and Promax (Halliburton) software for data processing. SPW from Parallel Geoscience was used for additional data processing. Seismic Micro Technology donated “the Kingdom Suite software” to all 4 involved universities, which we used extensively for interpretation and graphics. Lamont-Doherty Earth Observatory publication number 7507. Supported by National Science Foundation grants OCE-03-28118, OCE-09-28447, OCE-03-27273, and OCE-09-29063.

References

Aksu, A., Hiscott, R.N., Yaşar, D., 1999. Oscillating Quaternary water levels of the Marmara Sea and vigorous outflow into the Aegean Sea from the Marmara Sea–Black Sea drainage corridor. Marine Geology 153, 275–302.

Aksu, A.E., Calon, T.J., Hiscott, R.N., Yaşar, D., 2000. Anatomy of the North Anatolian fault zone in the Marmara Sea, western Turkey: extensional basins above a continental transform. GSA Today 10, 3–7.

Ambraseys, N., Finkel, C., 1995. The Seismicity of Turkey and Adjacent Areas 1500–1800. Eren Yayincilik ve Kitapcilik, Istanbul, Turkey. 240 pp.

Ambraseys, N.N., Jackson, J.A., 2000. Seismicity of the Sea of Marmara (Turkey) since 1500. Geophysical Journal International 141, F1–F6.

Armijo, R., Meyer, B., Hubert, A., Barka, A., 1999. Westward propagation of the north Anatolian fault into the northern Aegean: timing and kinematics. Geology 27, 267–270.

Armijo, R., Meyer, B., Navarro, S., King, G., Barka, A., 2002. Asymmetric slip partitioning in the Sea of Marmara pull-apart: a clue to propagation processes of the North Anatolian Fault? Terra Nova 14, 80–86.

Armijo, R., Pondard, N., Meyer, B., Uçarkus, G., Mercier de Lépinay, B., Malavieille, J., Dominguez, S., Gustcher, M.-A., Schmidt, S., Beck, C., Çagatay, N., Çakir, Z., İmren, C., Eris, K., Natalin, B., Özalaybey, S., Tolun, L., Lefèvre, I., Seeber, L., Gasperini, L., Rangin, C., Emre, O., Sarikavak, K., 2005. Submarine fault scarps in the Sea of Marmara pull-apart (North Anatolian Fault): implications for seismic hazard in Istanbul. Geochemistry, Geophysics, Geosystems 6, Q06009. doi:10.1029/2004GC000896.

Barka, A., 1996. Slip distribution along the North Anatolian Fault associated with the large earthquakes of the period 1939 to 1967. Bulletin of the Seismological Society of America 86, 1238–1254.

Barka, A.A., 1999. The 17 August 1999 Izmit earthquake. Science 285, 1858–1859.

Barka, A.A., Kadinsky-Cade, K., 1988. Strike-slip fault geometry in Turkey and its influence on earthquake activity. Tectonics 7, 663–684.

Bécel, A., Laigle, M., de Voogd, B., Hirn, A., Taymaz, T., Yolsal-Cevikbilen, S., Shimamura, H., 2010. North Marmara Trough architecture of basin infill, basement and faults, from PSDM reflection and OBS refraction seismics. Tectonophysics 490. doi:10.1016/j.tecto.2010.04.004.

Beck, C., Mercier de Lépinay, B., Schneider, J.-L., Cremer, M., Çağatay, N., Wendenbaum, E., Boutareaud, S., Ménot, G., Schmidt, S., Weber, O., Eris, K., Armijo, R., Meyer, B., Pondard, N., Gutscher, M.-A., MARMARACORE Cruise Party, Turion, J.-L., Labeyrie, L., Cortijo, E., Gallet, Y., Bouqueral, H., Görür, N., Gervais, A., Castera, M.-H., Londeix, L., de Resseguier, A., Jaouen, A., 2007. Late Quaternary co-seismic sedimentation in the Sea of Marmara's deep basins. Sedimentary Geology. doi:10.1016/j.sedgeo.2005.12.031.

Beşiktepe, Ş.T., Sur, H.İ., Özsoy, E., Latif, M.A., Oğuz, T., Ünlüata, Ü., 1994. The circulation and hydrography of the Marmara Sea. Progress in Oceanography 34, 284–334.

Brocher, T.M., 2005. Empirical relations between elastic wavespeeds and density in the earth's crust. Bulletin of the Seismological Society of America 95, 2081–2092. doi:10.1785/0120050077.

C&K Petroleum, 1974. Report Covering Geophysics — Geology Marmara Offshore, Turkey. 71 pp.

Çağatay, M.N., Eriş, K., Ryan, W.B.F., Sancar, Ü., Polonia, A., Akçer, S., Biltekin, D., Gasperini, L., Görür, N., Lericolais, G., Bard, E., 2009. Late Pleistocene-Holocene evolution of the northern shelf of the Sea of Marmara. Marine Geology 265, 87–100. doi:10.1016/j.margeo.2009.06.011.

Carton, H., Singh, S.C., Hirn, A., Bazin, S., de Voogd, B., Vigner, A., Richolleau, A., Cetin, S., Oçakoglu, N., Karakoç, F., Sevilgen, V., 2007. Seismic imaging of the three-dimensional architecture of the Çinarcik Basin along the North Anatolian Fault. Journal of Geophysical Research 112 http://www.ipgp.fr/~singh/DATA-SEISMARMARA/. doi:10.1029/2006JB004548.

Cormier, M.-H., Seeber, L., McHugh, C.M.G., Polonia, A., Çagatay, N., Emre, Ö., Gasperini, L., Görür, N., Bortoluzzi, G., Bonatti, E., Ryan, W.B.F., Newman, K.R., 2006. North Anatolian Fault in the Gulf of Izmit (Turkey): rapid vertical motion in response to minor bends of a nonvertical continental transform. Journal of Geophysical Research 111, B04102. doi:10.1029/2005JB003633.

Demirbağ, E., Rangin, C. Le, Pichon, X., Şengör, A.M.C., 2003. Investigation of the tectonics of the Main Marmara Fault by means of deep-towed seismic data. Tectonophysics 361, 1–19.

Dessa, J., Carton, H., Singh, S.C., 2007. Structural insight of the Eastern Marmara Sea by combined multichannel seismics and refraction tomography. Eos Trans. AGU 88 (52) Fall Meet. Suppl., Abstract T31C-0595..

Ergun, M., Ozel, E., 1995. Structural relationship between the Sea of Marmara Basin and the North Anatolian Fault Zone. Terra Nova 7, 278–288.

Erturaç, M.K., 2002, The coastal information system of the Marmara Sea (MARCIS), MSc Thesis (in Turkish). Istanbul Technical University, Eurasia Institute of Earth Sciences, Istanbul, 121 pp.

Gökaşan, E., Tur, H., Ergin, M., Görüm, T., Batuk, F.G., Sağci, N., Ustaömer, T., Emen, O., Alp, H., 2010. Late Quaternary evolution of the Çanakkale Straight region (Dardanelles, NW Turkey): implications of a major erosional event for the postglacial Mediterranean–Marmara Sea connection. Geo-Marine Letters 30, 113–131. doi:10.1007/s00367-009-0166-2.

Hubert-Ferrari, A., Barka, A., Jacques, E., Nalbant, S.S., Meyer, B., Armijo, R., Tapponnier, P., King, G.C.P., 2000. Seismic hazard in the Marmara Sea region following the 17 August 1999 Izmit earthquake. Nature 404, 269–273.

Hughes, D.R., 1985. V w/o T (velocity without tears). Geophysics: The Leading Edge of Exploration, pp. 50–52.

İmren, C., Le Pichon, X., Rangin, C., Demirbağ, E., Ecevitoğlu, B., Görür, N., 2001. The North Anatolian Fault within the Sea of Marmara: a new interpretation based on multi-channel seismic and multi-beam bathymetry data. Earth and Planetary Science Letters 186, 143–158.

Kansas Geological Survey, http://www.kgs.ku.edu/Tis/surf3/surf3Home.html.

Kazanci, N., Emre, Ö., Erkal, T., Ilieri, Ö., Ergin, M., Görür, N., 1999. Morphology and sedimentary facies of actual Kocasu and Gönen River deltas, Marmara Sea, Northwestern Anatolia. Mineral Research and Exploration Bulletin 121, 1–18.

Kozaci, O., Dolan, J., Finkel, R., Hartleb, R., 2007. Late Holocene slip rate for the North Anatolian fault, Turkey, from cosmogenic ^{36}Cl geochronology: implications for the constancy of fault loading and strain release rates. Geology 35, 867–870. doi:10.1130/G23187A.1.

Kurt, H., Sorlien, C.C., Seeber, L., Steckler, M.S., Shillington, D.J., Çifçi, G., Demirbağ, E., Cormier, M.-H., Atgin, O., Barin, B., Dondurur, D., İmren, C., Gürçay, S., Okay, S., 2011. Quaternary evolution of Cinarcik basin. Marmara Sea, Turkey, from structural and stratigraphic interpretation of multiple resolutions of seismic reflection data. *Eos Trans. AGU, 92, Fall Meet. Suppl.*, Abstract T31F-08.

Kuşçu, İ., 2009. Cross-basin faulting and extinction of pull-apart basins in the Sea of Marmara, NW Turkey. Turkish Journal of Earth Sciences 18, 331–349. doi:10.3906/yer-0706-4.

Kuşçu, İ., Okamura, M., Matsuoka, H., Yamamori, K., Awata, Y., Ozalp, S., 2009. Recognition of active faults and stepover geometry in Gemlik Bay, Sea of Marmara, NW Turkey. Marine Geology 260, 90–101. doi:10.1016/j.margeo.2009.02.003.

Laigle, M., Bécel, A., de Voogd, B., Hirn, A., Taymaz, T., Ozalaybey, S., Cetin, S., Galvé, A., Karabulut, H., Lépine, J.C., Saatçilar, R., Sapin, M., Shimamura, H., Murai, Y., Singh, S., Tan, O., Vigner, A., Yolsal, S., 2008. A first deep seismic survey of the Sea of Marmara: Deep basins and whole crust architecture and evolution. Earth and Planetary Science Letters. doi:10.1016/j.epsl.2008.02.031.

Le Pichon, X., Şengör, A.M.C., Demirbağ, E., Rangin, C., İmren, C., Armijo, R., Görür, N., Çağatay, N., Mercier de Lepinay, B., Meyer, B., Saatçilar, R., Tok, B., 2001. The active Main Marmara Fault. Earth and Planetary Science Letters 192, 595–616.

Le Pichon, X., Chamot-Rooke, N., Rangin, C., 2003. The North Anatolian fault in the Sea of Marmara. Journal of Geophysical Research 108. doi:10.1029/2002JB001862.

Lericolais, G., Henry, P., 2004. Cruise report of Marmara VT / Marmacore 2. http://www.cdf.u-3mrs.fr/~henry/marmara/marmaraVT.html2004.

Lisiecki, L.E., Raymo, M.E., 2005. A Pliocene–Pleistocene stack of 57 globally distributed benthic δ^{18}O records. Paleoceanography 20, PA1003. doi:10.1029/2004PA001071.

Marathon Petroleum Turkey Limited, 1975. Final Well Report Marmara No. 1. 138 pp.

McClusky, S., Balassanian, S., Barka, A., Demir, C., Ergintav, S., Georgiev, I., Gurkan, O., Hamburger, M., Hurst, K., Kahle, H., Kastens, K., Kekelidze, G., King, R., Kotzev, V., Lenk, O., Mahmoud, S., Mishin, A., Nadariya, M., Ouzounis, A., Paradissis, D., Peter, Y., Prilepin, M., Reilinger, R., Sanli, I., Seeger, H., Tealeb, A., Toksöz, M.N., Veis, G., 2000. Global positioning system constraints on plate kinematics and dynamics in the eastern Mediterranean and Caucasus. Journal of Geophysical Research 105, 5695–5719.

McHugh, C.M.G., Gurung, D., Giosan, L., Ryan, W.B.F., Mart, Y., Sancar, U., Burckle, L., Çağatay, M.N., 2008. The last reconnection of the Marmara Sea (Turkey) to the world ocean: a Paleoceanographic and paleoclimatic perspective. Marine Geology 255, 64–82.

Meade, B.J., Hager, B.H., McClusky, S.C., Reilinger, R.E., Ergintav, S., Lenk, O., Barka, A., Özener, H., 2002. Estimates of seismic potential in the Marmara Sea region from block models of secular deformation constrained by Global Positioning System measurements. Bulletin of the Seismological Society of America 92, 208–215.

Miller, K.G., Kominz, M.A., Browning, J.V., Wright, J.D., Mountain, G.S., Katz, M.E., Sugarman, P.J., Cramer, B.S., Christie-Blick, N., Pekar, S.F., 2005. The Phanerozoic record of sea-level change. Science 301, 1293–1298.

Okay, A.I., Demirbağ, E., Kurt, H., Okay, N., Kuşçu, İ., 1999. An active, deep marine strike-slip basin along the North Anatolian fault in Turkey. Tectonics 18, 129–147.

Okay, A.I., Kashlar-Özcan, A., İmren, C., Boztepe-Güney, A., Demirbağ, E., Kuşçu, İ., 2000. Active faults and evolving strike-slip basins in the Marmara Sea, northwest Turkey: a multichannel seismic reflection study. Tectonophysics 321, 189–218.

Okay, A.I., Tüysüz, O., Kaya, Ş., 2004. From transpression to transtension: changes in morphology and structure around a bend on the North Anatolian Fault in the Marmara region. Tectonophysics 391, 259–282.

Parke, J.R., White, R.S., McKenzie, D., Minshull, T.A., Bull, J.M., Kuşçu, İ., Görür, N., Şengör, C., 2002. Interaction between faulting and sedimentation in the Sea of Marmara, western Turkey. Journal of Geophysical Research 107, 2286. doi:10.1029/2001JB000450.

Parke, J.R., White, R.S., McKenzie, D., Minshull, T.A., Bull, J., Kuşçu, İ., Görür, N., Şengör, A.M.C., 2003. The Sea of Marmara: a two-dimensional seismic reflection data archive. Geochemistry, Geophysics, Geosystems 4, 1084. doi:10.1029/2002GC000493.

Parsons, T., 2004. Recalculated probability of M ≥ 7 earthquakes beneath the Sea of Marmara, Turkey. Journal of Geophysical Research 109. doi:10.1029/2003JB002667.

Parsons, T., Toda, S., Stein, R.S., Barka, A., Dieterich, J.H., 2000. Heightened odds of large earthquakes near Istanbul: an interaction-based probability calculation. Science 288, 661–665. doi:10.1126/science.288.5466.661.

Pinter, N., Sorlien, C.C., Scott, A.T., 2003. Fault-related fold growth and isostatic subsidence, California Channel Islands. American Journal of Science 303, 300–318.

Piper, D.J.W., Aksu, A.E., 1992. Architecture of stacked Quaternary deltas correlated with global oxygen isotopic curve. Geology 20, 415–418.

Plint, A.G., Nummedal, D., 2000. The falling stage systems tract: recognition and importance in sequence stratigraphic analysis. In: Hunt, D., Gawthorpe, R.L. (Eds.), Sedimentary Responses to Forced Regressions: London: Geol. Soc. Spec.Pub, 172, pp. 1–17.

Polonia, A., Gasperini, L., Amorosi, A., Bonatti, E., Bortoluzzi, G., Çağatay, N., Capotondi, L., Cormier, M.-H., Görür, N., McHugh, C., Seeber, L., 2004. Holocene slip rate of the North Anatolian Fault beneath the Sea of Marmara. Earth and Planetary Science Letters 227, 411–426.

Rangin, C., Demirbağ, E., İmren, C., Crusson, A., Normand, A., Le Drezen, E., Le Bot, A., 2001. Marine Atlas of the Sea of Marmara (Turkey). Ifremer Brest Technology Center, 11 Plates and 1 Booklet.

Rangin, C., Le Pichon, X., Demirbağ, E., İmren, C., 2004. Strain localization in the Sea of Marmara: propagation of the North Anatolian Fault in a now inactive pull-apart. Tectonics 23, TC2014. doi:10.1029/ 2002TC001437.

Reilinger, R.E., McClusky, S.C., Oral, M.B., King, R,.W., Toksoz, M.N., Barka, A.A., Kinik, I., Lenk, O., Sanli, I., 1997. Global Positioning System measurements of present-day crustal movements in the Arabia–Africa–Eurasia plate collision zone. Journal of Geophysical Research 102, 9983–9999.

Seeber, L., Emre, O., Cormier, M.-H., Sorlien, C.C., McHugh, C., Polonia, A., Ozer, N., Çağatay, N., The Team of the 2000 Urania Cruise in the Marmara Sea, 2004. Uplift and subsidence from oblique slip: the Ganos–Marmara bend on the North Anatolian Transform, Western Turkey. Tectonophysics 391, 239–258. doi:10.1016/j.tecto.2004.07.015.

Seeber, L., Cormier, M.-H., McHugh, C., Emre, O., Polonia, A., Sorlien, C., 2006. Rapid subsidence and sedimentation from oblique slip near a bend on the North Anatolian transform fault in the Marmara Sea, Turkey. Geology 34, 933–936. doi:10.1130/G22520A.

Seeber, L., Sorlien, C., Steckler, M., Cormier, M.-H., 2010. Continental transform basins: why are they asymmetric? EOS. Transactions of the American Geophysical Union 91, 29–31.

Sengör, A.M.C., Görür, N., Saroğlu, F., 1985. Strike-slip faulting and related basin formation in zones of tectonic escape: Turkey as a case study. In: Biddle, K.T., Christie-Blick, N. (Eds.), Strike-slip Deformation, Basin Formation, and Sedimentation: Soc. Econ. Paleontol. Miner. Spec. Publ., 37, pp. 227–264 (in honor of J.C. Crowell).

Sengör, A.M.C., Tüysüz, O., İmren, C., Sakınç, M., Eyidoğan, H., Görür, N., Le Pichon, X., Rangin, C., 2005. The North Anatolian Fault: a new look. Annual Review of Earth and Planetary Sciences 33, 37–112. doi:10.1146/annurev.earth.32.101802.120415.

Sheriff, R.E., 1973. Encyclopedic Dictionary of Exploration Geophysics. Society of Exploration Geophysicists, Tulsa, Okalahoma. 266 pp.

Shillington, D.J., Seeber, L., Sorlien, C.C., Steckler, M.S., Kurt, H., Dondurur, D., Çifçi, G., İmren, C., Cormier, M.-H., Gürçay, S., Poyraz, D.T., Okay, S., Diebold, J.B., Slow-motion collapse on the flanks of the Sea of Marmara transform basin. in review, Geology.

Smith, A.D., Taymaz, T., Oktay, F., Yüce, H., Alpar, B., Başaran, H., Jackson, J.A., Kara, S., Şimşek, M., 1995. High-resolution seismic profiling in the Sea of Marmara (northwest Turkey): Late Quaternary sedimentation and sea-level changes. Geological Society of America Bulletin 107, 923–936.

Stein, R.S., Dieterich, J.H., Barka, A.A., 1996. Role of stress triggering in earthquake migration on the North Anatolian Fault. Physics and Chemistry of the Earth 21, 225–230.

Toksoz, M.N., Shakal, A.F., Michael, A.J., 1979. Space–time migration of earthquakes along the North Anatolian fault zone and seismic gaps. Pure and Applied Geophysics 117, 1258–1270.

Tolmachoff, W., 1993. Linear velocity functions and the effect of mentors on the oil industry. Pac. Petr. Geol. Newsletter, Spring 1993. Pacific Section, Am. Assoc. Petr. Geol, pp. 4–5.

Wilcox, R.E., Harding, T.P., Seeley, D.R., 1973. Basic wrench tectonics. American Association of Petroleum Geologists Bulletin 57, 74–96.

Winker, C.D., Edwards, M.B., 1983. Unstable progradational clastic shelf margins. In: Stanley, D.J., Moore, G.T. (Eds.), The shelfbreak: critical interface on continental margins: Society of Economic Paleontologists and Mineralogists Special Publication, 33, pp. 139–156. Tulsa, Oklahoma.

Yaltirak, C., 2002. Tectonic evolution of the Marmara Sea and its surroundings. Marine Geology 3175, 1–38.

Yaltirak, C., Sakinç, M., Aksu, A.E., Hiscott, R.N., Galleb, B., Ulgen, U.B., 2002. Late Pleistocene uplift history along the southwestern Marmara Sea determined from raised coastal deposits and global sea-level variations. Marine Geology 190, 283–305.